

DETERMINATION OF THE LOSSES IN INDUCTION MACHINES  
DUE TO HARMONICS

by

Abdolmajid Banihaschemi

Diplom Ingenieur (M.S.), Technische Hochschule

Aachen, W. Germany, 1969

A REPORT SUBMITTED IN PARTIAL FULFILMENT  
OF THE REQUIREMENTS FOR THE DEGREE OF  
Master of Engineering  
in the Department  
of  
Electrical Engineering

This report is accepted.

Dean of Graduate Studies  
THE UNIVERSITY OF NEW BRUNSWICK  
OCTOBER, 1973

## ABSTRACT

This report is concerned with the determination of the stray load losses due to the higher harmonics in induction machines. The performance of the machine is also studied through a modified circle diagram. The I.E.E.E. "Test Code Procedure for Polyphase Induction Motors and Generators" has been used to determine the machine parameters and to calculate the performance of the machine. It has been found that the I.E.E.E. "Test Code Procedure for Polyphase Induction Motors and Generators" yields inaccurate results for the torque as well as the stray load losses. An alternative procedure, which gives better results has been presented. Several tests have been conducted to determine the stray load losses. The part of these losses due to the higher harmonics has been determined through the discrete Fourier series of the air-gap flux. It is shown that the higher harmonic losses represent a remarkable percentage of the total stray load losses, especially within the working range of the machine. Two methods of drawing the circle diagrams have been studied. The machine performance obtained from these methods shows close agreement between the computed and measured results.

## ACKNOWLEDGEMENT

The author wishes to thank Dr. B. Szabados for his guidance, encouragement and assistance throughout the course of this investigation and also for the financial support from the N.R.C. grants.

## TABLE OF CONTENTS

|   | Page |
|---|------|
| ABSTRACT .....  | ii   |
| ACKNOWLEDGEMENT .....   | iii  |
| LIST OF FIGURES .....   | viii |
| LIST OF TABLES .....  | x    |
| NOMENCLATURE .....  | xi   |
| <br>Chapter   |      |
| 1 INTRODUCTION .....  | 1    |
| 1.1 Historical Review .....   | 1    |
| 1.2 Proposed Work .....   | 3    |
| 2 METHOD OF PARAMETER DETERMINATION .....   | 5    |
| 2.1 Test Code Procedure .....   | 5    |
| 2.1.1 Steinmetz Equivalent Circuit .  | 5    |
| 2.1.2 Theoretical Background for<br>Test Procedure .....  | 9    |
| 2.2 Determination of Parameters and Per-<br>formance According to the I.E.E.E.<br>Test Code ..... | 11   |
| 2.2.1 Description of Tests .....  | 11   |
| 2.3 Comparison of Measured and Calculated<br>Performance .....                                    | 13   |
| 3 CONSIDERATION OF STRAY LOAD LOSSES .....  | 15   |
| 3.1 Definition of Stray Load Losses .....   | 15   |
| 3.2 Summary of Main Components of Stray<br>Losses .....   | 19   |
| 3.2.1 Surface Losses .....  | 21   |
| 3.2.2 Tooth-Pulsation Losses .....  | 21   |

| TABLE OF CONTENTS - continued                                | Page |
|--|------|
| 3.2.3 Slot-Leakage Flux (Stator Winding) Losses .....        | 22   |
| 3.2.4 Slot-Leakage Flux (Rotor Winding) Losses .....         | 22   |
| 3.2.5 Overhang-Leakage Flux (Stator Winding) Losses .....    | 22   |
| 3.2.6 Overhang-Leakage Flux (Rotor Winding) Losses .....     | 22   |
| 3.3 Methods of Determining Stray Load Losses .....           | 23   |
| 3.4 Description of Tests .....                               | 25   |
| 3.4.1 The Rawcliffe and Menon Test                           | 25   |
| 3.4.2 The Reverse Rotation Test ...                          | 27   |
| 3.4.3 The Ware's Test .....                                  | 31   |
| 3.5 Practical Application of Test Procedure .....            | 32   |
| 3.5.1 Reverse Rotation Test .....                            | 32   |
| 3.5.2 No-Load and Standstill Test .                          | 34   |
| 3.6 Determination of Stray Losses Due to the Harmonics ..... | 34   |
| 3.6.1 No-Load Condition .....                                | 35   |
| 3.6.2 Half-Load and Full-Load Conditions .....               | 36   |
| 3.7 Practical Application of Test Procedure .....            | 37   |
| 3.7.1 The Analysis of Harmonic Losses at No-Load .....       | 38   |
| 3.7.2 Stray Losses at Half-Load and Full-Load .....          | 42   |

## TABLE OF CONTENTS - continued

Page

|   |  |    |
|---|--|----|
|   | 3.7.3 The Analysis of Harmonic<br>Losses at Half-Load and<br>Full-Load ..... | 43 |
|   | 3.8 Some Aspects of Harmonic Analysis ..                                     | 45 |
| 4 | THE "EXACT" CIRCLE DIAGRAM OF THE<br>INDUCTION MOTORS .....                  | 54 |
|   | 4.1 Introduction .....   | 54 |
|   | 4.2 The First Method of Constructing the<br>"Exact" Circle Diagram .....     | 54 |
|   | 4.2.1 Theory .....   | 54 |
|   | 4.2.2 Equivalent Simplified Circuit  | 61 |
|   | 4.2.3 Construction of "Exact" Circle<br>Diagram from Design Data ....        | 63 |
|   | 4.2.4 Performance of the Motor ....  | 66 |
|   | 4.2.5 Construction of "Exact" Circle<br>Diagram from Test Data .....         | 68 |
|   | 4.3 Second Method of Determining the<br>"Exact" Circle Diagram .....         | 71 |
|   | 4.3.1 Inversion .....  | 71 |
|   | 4.3.2 The Impedance Diagram .....  | 74 |
|   | 4.3.3 The Admittance Diagram .....   | 76 |
|   | 4.4 Determination of the Parameters of<br>the Circle Diagram .....           | 79 |
|   | 4.4.1 Measurement of Blondel<br>Coefficient .....                            | 79 |
|   | 4.5 Influence of the No-Load Losses ....                                     | 82 |
|   | 4.6 Construction of the "Exact Circle"<br>Diagram from Test Data .....       | 83 |

| TABLE OF CONTENTS - continued |  | Page |
|-------------------------------|--|------|
|                               | 4.7 Calculation of Coordinates of Point $P_{\infty}$ .....       | 85   |
|                               | 4.8 Examples of Measurements and Interpretation of Results ..... | 89   |
| 5                             | SUMMARY AND CONCLUSIONS .....                                    | 97   |
|                               | 5.1 Summary .....  | 97   |
|                               | 5.2 Conclusion of First Part .....                               | 98   |
|                               | 5.3 Conclusion of Second Part .....                              | 102  |
| Appendix                      |  |      |
| I                             | SPECIFICATION OF MACHINE .....                                   | 104  |
| II                            | DISCRETE FOURIER SERIES .....                                    | 105  |
|                               | REFERENCES .....   | 109  |

## LIST OF FIGURES

| Figure |   | Page |
|--------|---|------|
| 2.1    | Equivalent Circuit of the Transformer .....                   | 7    |
| 2.2    | Phasor Diagram of Induction Motor .....                       | 7    |
| 2.3    | Equivalent Circuit of the Induction Motor                     | 10   |
| 3.1    | Mechanism of Losses due to the Tooth<br>Ripples .....         | 17   |
| 3.2    | Typical $sV_1^2$ versus Voltage Curve .....                   | 28   |
| 3.3    | No-Load Condition .....                                       | 35   |
| 3.4    | Half-Load and Full-Load Conditions .....                      | 37   |
| 3.5    | Per Unit Torque versus Slip .....                             | 49   |
| 3.6    | Air-Gap Flux at No-Load .....                                 | 50   |
| 3.7    | Air-Gap Flux at Full-Load .....                               | 51   |
| 3.8    | Air-Gap Flux and Discrete Line Spectrum<br>at No-Load .....   | 52   |
| 3.9    | Air-Gap Flux and Discrete Line Spectrum<br>at Full-Load ..... | 53   |
| 4.1    | Equivalent Circuit of the Induction Motor                     | 55   |
| 4.2    | Thevenin's Circuit .....                                      | 56   |
| 4.3    | Vector Diagram at No-Load .....                               | 59   |
| 4.4    | Representation of Primary and Magnetizing<br>Currents .....   | 60   |
| 4.5    | Equivalent Simplified Circuit .....                           | 63   |
| 4.6    | The Exact Circle Diagram of the Induction<br>Motor .....      | 65   |
| 4.7    | Determination of Performance .....                            | 69   |
| 4.8    | Construction of the Circle Diagram from<br>Test Data .....    | 72   |



# LIST OF FIGURES - continued

| Figure |   | Page |
|--------|---|------|
| 4.9    | Inversion of Straight Line and Circle .....   | 73   |
| 4.10   | The Impedance Diagram .....   | 75   |
| 4.11   | Inversion of Impedance to Admittance<br>Diagram .....   | 80   |
| 4.12   | Separation of No-Load Losses .....  | 83   |
| 4.13   | Construction of the Circle Diagram .....  | 88   |
| 4.14   | Construction of the Circle Diagram from<br>Test Data of the Induction Machine by the<br>First Method .....  | 91   |
| 4.15   | Construction of the Circle Diagram from<br>Test Data of the Induction Machine by the<br>Second Method ..... | 92   |
| 4.16   | Per Unit Torque versus Slip .....   | 93   |
| 4.17   | Per Unit Stator Current versus Slip .....   | 94   |
| 4.18   | Per Unit Input Power versus Slip .....  | 95   |
| 4.19   | Power Factor versus Slip .....  | 96   |

## LIST OF TABLES

| Table |  | Page |
|-------|--|------|
| 2.1   | Tabulation of Test Data .....                                  | 14   |
| 2.2   | Parameters from Test Code Procedure .....                      | 14   |
| 3.1   | Summary of Stray Loss Components .....                         | 20   |
| 3.2   | Test Data at No-Load from Various Methods                      | 42   |
| 3.3   | Test Data at Half-Load from Various<br>Methods .....           | 43   |
| 3.4   | Test Data at Full-Load from Various<br>Methods .....           | 44   |
| 3.5   | Components of Stray Losses and Suggested<br>Measurements ..... | 46   |
| 4.1   | Tabulation of Test Data .....                                  | 71   |
| 4.2   | Tabulation of Test Data .....                                  | 90   |

## NOMENCLATURE

|          |  |
|----------|--|
| $V_1$    | stator applied voltage   |
| $I_1$    | stator current   |
| $E_1$    | primary developed voltage due to the air-gap field                 |
| $E_{NL}$ | value of $E_1$ at no-load  |
| $E_2$    | secondary developed voltage due to air-gap field                   |
| $R_1$    | stator resistance at operating temperature                         |
| $X_1$    | stator leakage reactance   |
| $Z_1$    | $R_1 + jX_1 =$ stator impedance                                    |
|          | reluctance of the core   |
| $s$      | slip   |
| $n_s$    | synchronous speed  |
| $n_o$    | $(1-s)n_s =$ speed   |
| $R_2$    | rotor resistance referred to primary impedance level               |
| $X_2$    | rotor leakage reactance referred to primary impedance level        |
| $Z_2$    | $R_2 + jX_2 =$ rotor impedance referred to primary impedance level |
| $I_2$    | rotor current  |
| $R'_1$   | stator resistance at temperatures during no-load tests             |
| $R''_1$  | stator resistance at temperatures during impedance tests           |
| $R_m$    | magnetizing resistance   |
| $X_m$    | magnetizing reactance  |
| $Z_m$    | $R_m + jX_m =$ magnetizing impedance                               |

|           |  |
|-----------|--|
| $Z_{SC}$  | locked rotor impedance   |
| $V_{SC}$  | line to line stator voltage during locked rotor test                                       |
| $I_{SC}$  | stator current during locked rotor test  |
| $W_{SC}$  | total three phase input power during locked rotor test                                     |
| $I_{NL}$  | stator current during no-load test   |
| $W_{NL}$  | total three phase input power during no-load test  |
| $N_1$     | number of turns in series in the stator  |
| $N_2$     | number of turns in series in the rotor   |
| $n$       | $\frac{N_2}{N_1} = \text{turns ratio}$   |
| $W_h$     | total three phase core loss  |
| $P_{fs}$  | total three phase stator core loss   |
| $P_m$     | total three phase friction and windage loss  |
| $P_{fr}$  | total three phase rotor core loss  |
| $LL_r$    | three phase fundamental frequency stray load loss  |
| $LL_s$    | three phase high frequency stray load loss   |
| $P_{st}$  | $LL_r + LL_s = \text{total three phase stray load loss}$                                   |
| $f$       | operating frequency  |
| $f_m$     | highest frequency by sampling  |
| $I_r$     | test stator current during reverse rotation test at rated load current                     |
| $H$       | value of stray load loss measured during the reverse rotation test at stator current $I_r$ |
| $I_m$     | magnetizing current  |
| $I_{e+h}$ | hysteresis and eddy current  |
| $K$       | $\frac{Z_m}{Z_1 + Z_m} = \frac{ Z_m }{ Z_1 + Z_m } (\cos \alpha + j \sin \alpha)$          |
| $\phi_m$  | air-gap (mutual) flux  |

|          |                                       |
|----------|---------------------------------------|
| $\phi_1$ | stator leakage flux                   |
| $\phi_2$ | rotor leakage flux                    |
| $K_d$    | distribution factor                   |
| $K_e$    | coil-span factor                      |
| $m$      | number of phases                      |
| $\sigma$ | Blondel coefficient                   |
| $\eta$   | efficiency                            |
| $X_M$    | mutual impedance from stator to rotor |
| $f_t$    | test frequency                        |

## CHAPTER 1

### INTRODUCTION

#### 1.1 Historical Review

With the help of transformer theory, C.P. Steinmetz [1] derived an equivalent circuit to represent the induction motor by assigning values for primary admittance on open secondary (associated with flux of mutual induction), primary impedance (associated with flux of self induction) and secondary impedance referred to the primary and he was able to calculate the performance of the machine using a characteristic constant. This constant allowed for treatment of magnetizing quantities and their effect. Some of the works published for determination of induction machine performance, were based on circle diagram and some were based on equivalent circuit. The interest in separating various losses in the induction machines arose with a view to determine the efficiency and the output of the machines. The term stray losses was discussed in the early works [2, 3, 4, 5, 6] with an attempt to correlate these losses with the discrepancies between actual and calculated efficiencies.

T. Sponner published in 1929 a paper [7] on induction motor core losses at no-load. He attempted to separate these losses into fundamental frequency losses in the

stator core and teeth, and higher frequency losses due to surface pulsation losses and eddy current copper losses. Based on Sponner's work C.J. Koch presented in 1932 [8] a new method to measure stray load losses. This method consisted in applying direct current to either primary or secondary with the other circuit shorted, driving the machine at synchronous speed and measuring the driving power. Subtraction of friction, windage and copper losses of the unexcited circuit yields the stray losses. This method is still accepted by the I.E.E.E. test code for measuring the stray losses in wound rotor machines.

Subsequent works [9] and [10] resulted in a new method [11] of determination of the stray load losses: the reverse rotation test, also accepted by the I.E.E.E. test code. By this method, a reduced polyphase voltage is applied to the machine driven at synchronous speed in the reverse direction by a coupled d.c. machine. Both a.c. and d.c. powers are measured and corrected for stator  $I^2R$  losses. The difference yields the stray load losses.

A paper by Rawcliffe and Menon [12] explains a new test for measuring the harmonic-frequency losses as a separate quantity in slip-ring or squirrel-cage motors. This test determines the higher harmonic losses at no-load.

Two papers by Barton and Ahmad [13] and [14] include intensive study about the nature of stray losses and their measurements. They suggest three sources of stray losses, eddy-current and iron losses at the supply frequency, tooth ripple in the main flux and tooth ripple in the zigzag leakage flux. In these papers the results of the reverse rotation test has been extrapolated from current and speed in order to calculate the stray losses over the wide speed range.

Early works on determining the machine performance by using the circle diagram theory were involved with elaborate geometrical constructions. P.K. Sattler [15], K.P. Kovacs [16] and A. Langsdorf [17] introduced graphical methods which simplified the calculation and construction of the exact circle diagram.

## 1.2 Proposed Work

This report proposes to assess the existing methods for determination of the stray losses and to investigate those losses due to the harmonic content in the air-gap flux. A Fourier analysis of the air-gap flux will determine the harmonic e.m.f.'s in the stator winding which allow the calculation of the higher harmonic losses as a part of the total stray losses. In addition a study of the circle diagram theory will be conducted and a modified



method proposed leading to more accuracy and more simplicity. The machine performance will then be compared to a model obtained from test code procedure. Finally an attempt will be made to look into the non-linearity of the inductive part related to Blondel's coefficient of leakage.

## CHAPTER 2

### METHOD OF PARAMETER DETERMINATION

#### 2.1 Test Code Procedure

##### 2.1.1 Steinmetz Equivalent Circuit

The original Steinmetz equivalent circuit [1] is the basic equivalent circuit employed in the procedure approved by the I.E.E.E. test code. Starting with basic theory the m.m.f. relationship in a transformer is as follows:

$$N_1 I_{NL} + N_1 I_1 + N_2 I_2 = \phi \lambda \quad (2.1)$$

where

$N_1$  = number of turns in primary coil

$N_2$  = number of turns in secondary coil

$I_{NL}$  = magnetizing or no-load current

$I_1$  = primary current

$I_2$  = secondary current

$\phi$  = core flux

$\lambda$  = reluctance of core

When the steady state is reached,  $I_{NL} N_1 = \phi \lambda$  and  $I_1 N_1 = I_2 N_2$  or  $I_1 = n I_2$ .

Then the following relations are obtained:

$$V_1 = I_1 (R_1 + jX_1) + j(I_1 - I_2)X_m + (I_1 - I_2)R_m \quad (2.2)$$

$$E_1 = j(I_1 - I_2)X_m - I_2(R_2 + jX_2) + (I_1 - I_2)R_m \quad (2.3)$$

These equations do not represent any effects of hysteresis and eddy current losses in the core. Since the real component of the magnetizing impedance is very much less than the imaginary one, it is neglected. These relations yield to the equivalent circuit of the transformer shown in Fig. 2.1. From equation (2.1), it is seen that  $N_1 I_{NL}$  provides only approximately the magnetizing magnetomotive force to produce a flux  $\phi_m$  in the core, and remains constant regardless of load. Since the core is subject to a constant magnetizing m.m.f. the magnetizing conductance may be included as a parallel branch.

The induction motor could be logically considered to be a transformer with a split core, the air-gap representing the space between the two parts.

Considering the analogy and examining equations (2.2), and (2.3), the phasor diagram for each phase of the induction motor with symmetrical phase windings and a balanced polyphase power supply may be drawn as shown in Figure 2.2. In Figure 2.2,  $V_1$  is the impressed voltage, and  $I_1$  the primary current phasor, lagging the voltage by an angle  $\theta_1$ . The secondary voltage, due to the air-gap field,  $E_2 = -E_1$ , is found by vectorial subtraction of the primary resistance drop,  $I_1 R_1$  and the primary leakage reactance drop,  $jI_1 X_1$ , for the impressed voltage.

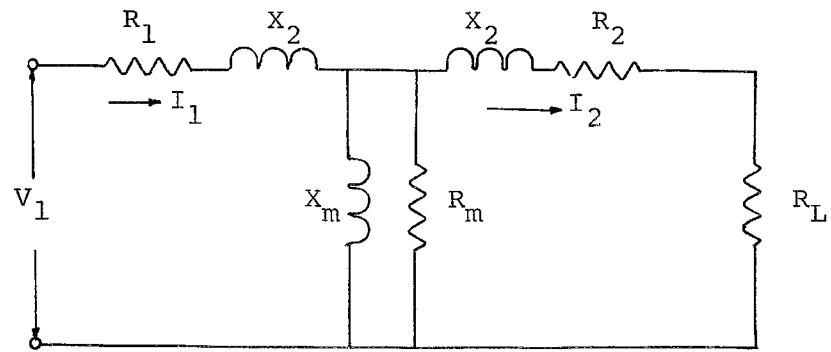


Figure 2.1 Equivalent Circuit of a Transformer

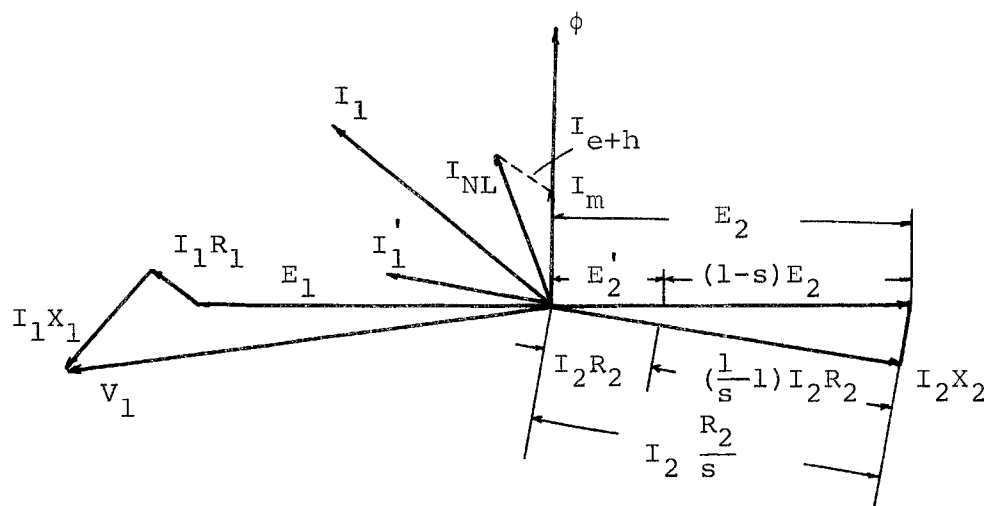


Figure 2.2 Phasor Diagram of Induction Motor

Since the rotor conductors are actually slipping with respect to the stator conductors at slip frequency, the actual voltage induced in the secondary is  $E_2' = s E_2$  and is entirely consumed in the secondary impedance drop, composed of  $\frac{I_2 R_2}{s}$  and  $I_2 X_2$ . In other words, considering the motor at standstill when  $s = 1$

$$I_2 = \frac{E_2}{R_2 + jX_2} \quad (2.4)$$

When the motor is running at slip  $s$

$$I_2 = \frac{E_2}{\frac{R_2}{s} + jX_2} \quad (2.5)$$

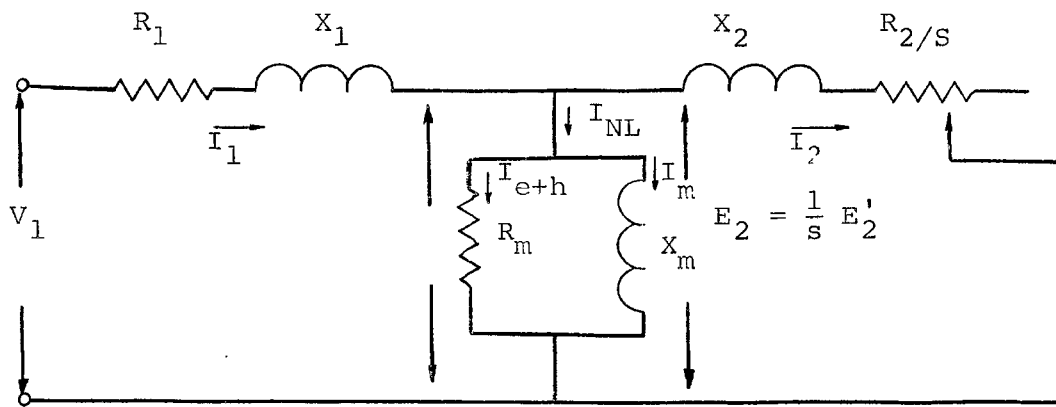
From the above equation it is evident that the apparent secondary resistance which seems to vary inversely with the slip could be considered as the sum of the actual resistance,  $R_2$ , and the load resistance  $R_2(1-s)/s$ . The phasor diagram further clarifies this because the standstill voltage developed across the apparent secondary resistance is actually partially used on loading to develop the voltage  $I_2 R_2(1-s)/s$ , across the load resistance. This is actually the part of the secondary voltage drop which is used to produce torque. Hence the transformer equivalent circuit is applicable if the load resistance,  $R_L$ , is replaced by the load resistance  $R_2(1-s)/s$ . This yields the equivalent circuit shown in Figure 2.3(a), which is the equivalent circuit used in

the I.E.E.E. test code.

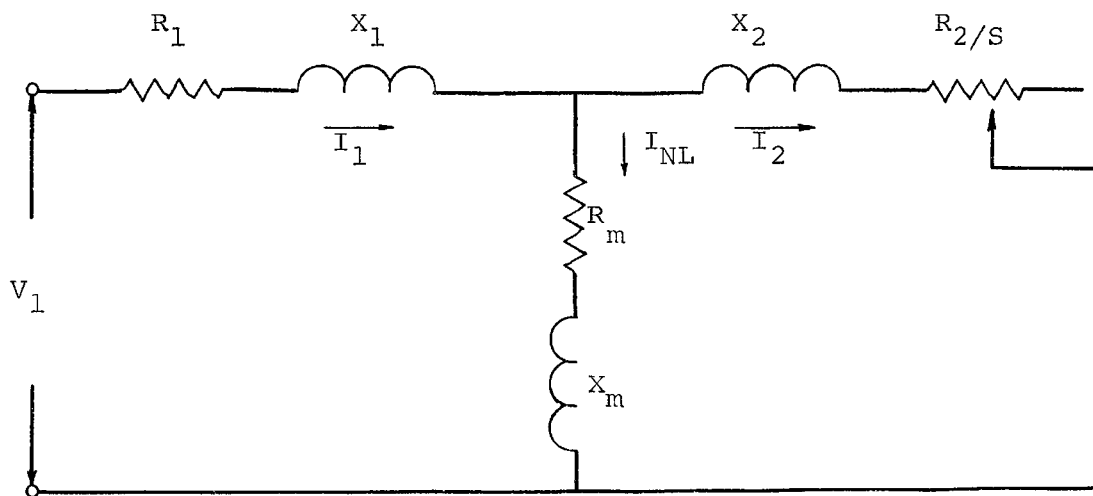
To produce the air-gap voltage,  $E_1$ , a magnetic flux,  $\phi$ , is required which lags  $E_1$  by  $90^\circ$ . A magnetizing current,  $I_m$ , is required to produce this flux, which together with the small hysteresis and eddy current,  $I_{e+h}$ , required to supply the core losses, must be subtracted from the primary current,  $I_1$ , to obtain the primary load current,  $I_1'$ . This in turn is equal and opposite to the secondary current  $I_2$ . In the exact equivalent circuit the core loss is represented by a copper loss in a fictitious resistance,  $R_m$ . This resistance, in parallel with the magnetizing reactance, makes the core loss vary with the flux which crosses the air-gap and consequently falls off as the load increases, but at the same time the core loss increases in the rotor.

### 2.1.2 Theoretical Background for Test Procedure

As recommended in the I.E.E.E. test code, the no-load test is done by running the machine at rated voltage and frequency without connected load. The input power, voltage and current are read. Having obtained the stator resistance from a d.c. resistance measurement, the stator copper loss at the temperature of the no-load test may be obtained. Subtracting this from the input gives the sum of the friction and windage and core loss. The locked rotor test consists of a series of readings of



(a) The Conventional Equivalent Circuit for the Induction Motor



(b) Another form of the Equivalent Circuit for the Induction Machine

Figure 2.3 Equivalent Circuit for an Induction Motor

voltage, current and power taken at different values of current, with the rotor blocked and short circuited, the frequency of the applied voltage being constant. For a wound rotor machine, it is necessary to block at a position corresponding to the average of its maximum and minimum input impedance positions.

Referring to the nomenclature used in this report, the parameters of the machine under test may be obtained from the following relations:

$$(X_1 + X_2) = \frac{f}{f_t} \sqrt{\frac{V_{SC}^2}{3I_{SC}^2} - \left(\frac{W_{SC}}{3I_{SC}^2}\right)^2} \quad (2.6)$$

$$R_2 = \left[ \frac{W_{SC}}{3I_{SC}^2} - R_1'' \right] * \frac{R_1}{R_1''} \quad (2.7)$$

$$W_h + P_m = W_{NL} - 3I_{NL}^2 R_1' \quad (2.8)$$

$$X_m = \frac{E_{NL}}{I_{NL}} \quad (2.9)$$

## 2.2 Determination of Parameters and Performance According to the I.E.E.E. Test Code

### 2.2.1 Description of Tests

The no-load test is made by running the machine at rated voltage and frequency without connected load. To insure that the correct value of friction and windage is



obtained, the machine should be operated until the input becomes constant. The temperature variation during these tests was measured through the use of embedded thermocouples in the winding slots of the machine. Ambient temperature was recorded as the average of the readings from two glass bulb mercury thermometers placed at various locations around the test set. Both stator and rotor resistance were measured by ammeter and voltmeter method. This method is used for the measurement of low resistance when an accuracy of the order of 1 percent is sufficient.

The reading of input watts is the total of the losses in the motor at no-load. Subtracting the stator  $I^2R$ -loss (at temperature of this test) from the input gives the sum of the friction (including brush friction loss on wound-rotor motors) and windage and core loss.

The separation may be made by reading volts, amperes, and watts input at rated frequency and at voltages ranging from 125 percent of rated voltage down to the point where further reduction increases the current. A curve of watts input versus voltage is plotted and the curve so obtained is extended to zero voltage. The intercept with zero voltage axis is the friction and windage loss. The intercept may be determined more accurately if the input is plotted against the voltage squared for values in the lower voltage range.

The locked rotor test was done at rated frequency.

The maximum and minimum impedance positions of the rotor were determined by applying reduced voltage to the stator and slowly turning the rotor position as close as practical to the average of the minimum and maximum current position. Having locked the rotor in the desired position, the required readings were taken as quickly as possible to avoid overheating. The summary of the test results for the machine is given in tabular form in Table 2.1. Using this data along with the relations stated in Section 2.1.2 and with those in "Test Code Procedure", the parameters of the machine were calculated. A summary of the parameters according to this method is given in Table 2.2. These parameters are shown for a winding temperature of  $45^{\circ}\text{C}$ .

### 2.3 Comparison of Measured and Calculated Performance

Using the parameters tabulated in Table 2.2 the torque-slip, input power-slip, power factor-slip, and stator current-slip were computed by the method F explained in the "Test Code Procedure". The performance curves for the same temperature were measured. The measured and calculated torque-slip, input power-slip, stator current-slip and power factor-slip are plotted at the end of Chapter 4.

The consequence of the stray loss correction is shown on a torque-slip curve, by plotting the curve both with and without stray loss included.

The torque-slip curve was computed using the modified expression for stray loss. This expression is explained in Section 3.1.

| No-Load Test Data                    |                                     |                              |   |
|--------------------------------------|-------------------------------------|------------------------------|---|
| Line Current<br>$I_{NL}$<br>(Ampere) | Line Voltage<br>$V_{NL}$<br>(Volts) | Power<br>$W_{NL}$<br>(Watts) | Winding<br>Temperature<br>( $^{\circ}C$ ) |
| 5.75                                 | 208                                 | 392                          | 29.15                                     |
| Locked Rotor Test Data               |                                     |                              |   |
| Line Current<br>$I_{SC}$<br>(Ampere) | Line Voltage<br>$V_{SC}$<br>(Volts) | Power<br>$W_{SC}$<br>(Watts) | Winding<br>Temperature<br>( $^{\circ}C$ ) |
| 10.80                                | 42.3                                | 379                          | 40  |

Table 2.1 Tabulation of Test Data

|       |            |          |             |
|-------|------------|----------|-------------|
| $R_1$ | 0.404 Ohms | $X_1$    | 1.08 Ohms   |
| $R_2$ | 0.626 Ohms | $X_2$    | 1.08 Ohms   |
| $R_m$ | 1.30 Ohms  | $X_m$    | 19.80 Ohms  |
| $P_m$ | 216 Watts  | H        | 35.46 Watts |
| $I_r$ | 8.7 Ampere | $\sigma$ | 0.103       |

Table 2.2 Parameters from Test Code Procedure

## CHAPTER 3

### CONSIDERATION OF STRAY LOAD LOSSES

#### 3.1 Definition of Stray Load Losses

According to the I.E.E.E. test code, stray losses are the part of the total losses in a machine which are not accounted for by the sum of friction and windage stator, rotor copper and no-load core losses. Considering the no-load core loss of an induction motor, a paper [5] by Spooner and Kinnard divided the core losses into the following components:

1. Fundamental frequency losses
  - (a) Stator core
  - (b) Stator tooth
2. Pulsation losses
  - (a) Surface (stator and rotor)
  - (b) Tooth pulsation (stator and rotor)
  - (c) Copper eddy (stator and rotor).

The fundamental frequency losses are those due to the hysteresis and eddy current losses in the core material corresponding to the applied frequency. The pulsation losses consist first, of the surface losses which are hysteresis and eddy current losses occurring below the surface of the tooth tops due to the passage of the slots of the other member and are practically the

same as the well known pole-face losses.

The tooth pulsation losses are caused by the high frequency pulsations of flux extending the whole length of the teeth and into the core due to the reluctance changes in the air-gap as the slots of one member pass the teeth of the other.

The eddy-current losses are not really core losses but appear as such by the ordinary methods of test. They are due to the high frequency slot-leakage fluxes as the result of the momentary changes in the saturation of the teeth.

A published paper by Koch [8] noted that the stray loss is the tooth frequency core loss which changes with load and that its increase with load constitutes a real reason for the observed stray load loss. He explained this by considering the losses in the rotor surface and teeth of a slip-ring induction motor. These are induced by the stator tooth harmonic flux. This flux may be considered as consisting of two component fluxes. The first of these is independent of load and is the harmonic flux produced by the action of the fundamental m.m.f. on the stator slot openings. The second varies with load and is due to the teeth harmonic m.m.f. produced by the concentration of the stator current in slots. It is the increase of this tooth harmonic m.m.f. with load

which accounts for the change of the tooth frequency core loss with load.

Barton and Ahmad suggested in [13] three sources of stray load losses in induction motors, eddy-current and iron losses at the supply frequency, tooth ripples in the main and tooth ripples in the zigzag leakage flux. Figure 3.1 illustrates the mechanism of losses due to the tooth ripples.

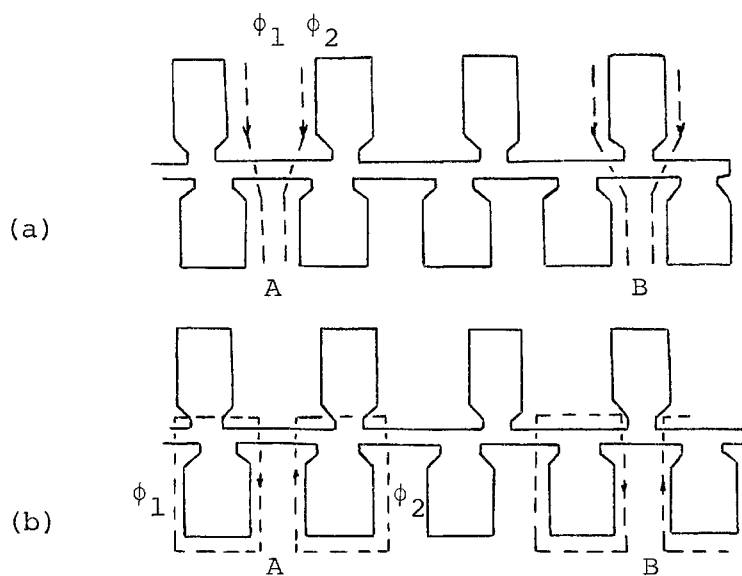


Figure 3.1 (a) Effect on the Main Flux

(b) Effect on the Zigzag Leakage Flux

It shows the stator and rotor teeth in various relative positions. Figure 3.1(a) shows the disposition of the main flux with the flux passing down the tooth A being

a maximum whilst that down B is a minimum. It is this variation of tooth flux at slot ripple frequency which is responsible for the voltage-dependent component of the stray loss. Figure 3.1(b) shows the zigzag leakage flux. Unless the stator and rotor pitches are equal, the variations of  $\phi_1$  and  $\phi_2$  are not in phase and there is a resultant variation of tooth flux at the tooth ripple frequency which is responsible for the current-dependent component of stray loss.

Both authors maintain that the stray loss associated with the tooth ripple in the main flux is small compared with that associated with the tooth ripple in the zigzag leakage flux, except at very small slips. The loss due to the tooth ripple in the main flux has three components:

- (1) The loss due to flux-density variation in the air-gap surfaces of the lamination.
- (2) The loss due to pulsations in the tooth fluxes.
- (3) The loss due to high frequency circulating currents in a squirrel-cage winding. The latter component has the effect of damping the flux pulsations in the rotor teeth and correspondingly increasing the pulsations in the stator teeth.

There is an important difference between the losses due to tooth harmonics and those due to tooth pulsations. Tooth pulsation losses are due to change of air-gap reluctance, and are approximately proportional to the

square of the fundamental mutual flux. Since the fundamental mutual flux does not change appreciably with load, the tooth pulsation losses remain practically constant throughout the loading. The tooth harmonic losses are due to the zigzag nature of the stator and rotor m.m.f., as demonstrated in Figure 3.1(b). While the fundamental component of the stator and rotor m.m.f. are essentially opposite to each other, with only enough left for magnetization, the tooth harmonics of both are unopposed. Thus the harmonic flux so induced is approximately proportional to the stator current, with the associated losses proportional to the square of stator current.

The experimental results of the investigation by Barton and Admad [14] describe that the zigzag flux component of the loss varies with (current)<sup>1.9</sup> and (speed)<sup>1.6</sup>. Therefore the expression for the stray loss becomes

$$P_{st} = H \left( \frac{n_o}{n_s} \right)^{1.6} \left( \frac{I_1}{I_r} \right)^{1.9} \quad (3.1)$$

where  $H$  and  $I_r$  are the stray loss power and current from reverse rotation test at rated load.

### 3.2 Summary of Main Components of Stray Losses

Table 3.1 shows the main individual components of stray losses segregated according to their dependence on main flux variations or leakage flux as discussed in previous sections.



| Class                                     | Component                           | Origin   | Type and Location                   |
|---|-------------------------------------|--|-------------------------------------|
| <u>A Main flux variation stray losses</u> |                                     |  |                                     |
| 1 a and b                                 | Surface losses                      | Permeance variation (harmonic flux)                | Stator and rotor core losses        |
| 2 a and b                                 | Tooth-pulsation losses              | Permeance variation due to relative tooth position | Stator and rotor core losses        |
| <u>B Leakage flux stray losses</u>        |                                     |  |                                     |
| 3 a and b                                 | Surface losses                      | Zigzag leakage (harmonic flux)                     | Stator and rotor core losses        |
| 4 a and b                                 | Tooth-pulsation losses              | Zigzag leakage (harmonic flux)                     | Stator and rotor core losses        |
| 5 a and b                                 | Stator-slot eddy-current losses     | Slot leakage flux                                  | Stator $I^2R$ loss                  |
| 6 a and b                                 | Rotor-slot eddy-current losses      | Slot leakage flux                                  | Rotor $I^2R$ loss at high slip only |
| 7 a and b                                 | Stator-overhang eddy-current losses | Overhang leakage flux                              | Stator core loss                    |
| 8 a and b                                 | Rotor-overhang eddy-current losses  | Overhang leakage flux                              | Rotor core loss at high slip        |

Table 3.1 Summary of Stray Loss Components

### 3.2.1 Surface Losses

These are additional core losses occurring on the stator and rotor surfaces owing to rotation, and the fluxes causing them are:

(a) The air-gap harmonics, due to tooth ripple variations of the main flux

(b) The air-gap zigzag leakage harmonic fluxes. The losses are dependent in a complex manner on the slotting, air-gap configuration and slot numbers. As the losses are caused mainly by high frequency eddy currents, those due to the main flux will vary as the square of the applied voltage and those due to the zigzag leakage flux will vary as the square of current.

### 3.2.2 Tooth-Pulsation Losses

These losses of the main and zigzag leakage flux harmonics are caused by the relative movement of the stator and rotor teeth, given rise to additional core losses in the stator and rotor teeth which are conditioned by the slot configuration air-gap and slot numbers. The magnitude of these fluxes is largely dependent on the saturation in the teeth, so that, although the losses are again substantially eddy-current losses, the variation is no longer proportional to the square of the voltage or current for the main flux variation and leakage flux stray losses.

### 3.2.3 Slot-Leakage Flux (Stator Winding) Losses

The slot leakage flux, i.e. the flux due to the self inductance in the embedded part of the winding, causes additional main frequency eddy-current losses in the winding, which are dependent on the square of the exciting current.

### 3.2.4 Slot-Leakage Flux (Rotor Winding) Losses

The effects mentioned in Section 3.2.3 occur in any squirrel-cage rotor at high slip, e.g. at start, but not during normal operation where, owing to the low frequency, no additional losses are incurred although the flux is present. These losses depend on the square of the current and vary in a complex manner with frequency and the shape and size of the conductors.

### 3.2.5 Overhang-Leakage Flux (Stator Winding) Losses

The stator winding overhang leakage flux may be partly linked with structural parts, resulting in main frequency eddy-current losses in these structures. These losses vary basically as the square of the current.

### 3.2.6 Overhang-Leakage Flux (Rotor Winding) Losses

The rotor winding behaves in exactly the same way as the stator winding, and stray load losses occur at high slip, i.e. high frequency.

### 3.3 Methods of Determining Stray Load Losses

The early method for measurement of stray losses consisted in measuring input and output powers and subtracting copper, friction and windage and core losses from the difference in order to obtain the stray losses.

An investigation of stray loss by Koch [8] resulted in the formulation of a test to directly measure stray losses. This test is still acknowledged by I.E.E.E. as an acceptable one for wound rotor motors. It consists of exciting the rotor with direct current while the stator terminals are short circuited. The rotor is driven by external means at synchronous speed. The rotational power minus friction and windage and copper losses yield to the stray load loss. A paper [9] by Morgan and Narbutoskish offered an alternative method for measuring stray load loss. By this method, which is still accepted by I.E.E.E. for both wound rotor and squirrel-cage machines, two similar machines were connected by means of an ordinary belt drive in such a manner that one acting as a motor drove the other as a generator. When connected to a common power line the total losses of the combination were measured as power input to the system. The losses usually considered in calculating conventional efficiency and belt losses were subtracted from the total losses giving a value which is the sum of the stray losses in both machines. Losses are apportioned

between motor and generator according to the ratio of their copper losses. This method suffers from its complexity and the necessity for duplicate machines.

There are two alternatives for measuring the fundamental-frequency stray losses.

(a) The standstill test [12]

(b) War's test [18], in which the power input to the stator, with polyphase excitation at the normal frequency, is measured with rotor removed. The reverse rotation test [11] allows the measurement of stray losses associated with the tooth ripple in the zigzag flux. Hence this test reproduces all losses listed in Table 3.1, classes 3-8. For determining the higher frequency losses at no-load there are also two alternatives.

(a) The Rawcliffe and Menon test [12] which measures all losses dependent on the tooth ripple in the main flux.

(b) No-load and standstill tests. The no-load test measures (fundamental iron loss and total harmonic losses) and the standstill test yields the fundamental iron loss. Hence higher harmonic losses could be calculated very easily. The harmonic analysis allows the determination of a part of higher harmonic losses in class 1 of Table 3.1 if search coils are mounted in the machine under test for measuring the main flux directly.

### 3.4 Description of Tests

#### 3.4.1 The Rawcliffe and Menon Test

This test consists in running the machine on no-load and measuring the total input power, slip and voltage over a wide voltage range consistent with the slip being extremely small. The power transferred to the rotor of an induction motor by action of primary field on the secondary windings is given by

$$P = \frac{msV_1^2 R_2}{(sR_1 + R_2)^2 + s^2 X^2} \text{ watts} \quad (3.2)$$

where  $m$  is the number of phases,  $s$  the fractional slip,  $R_1$  the primary resistance per phase,  $R_2$  the secondary referred resistance per phase, and  $X$  the total inductance referred to the stator. No-load fractional slip rarely exceeds 0.005, even on considerably reduced voltage.

Hence, to a very high degree of accuracy, the denominator of the above expression is equal to  $R_2^2$  and the resultant expression is

$$P_{\text{tran}} \approx \frac{msV_1^2}{R_2} \text{ watts} \quad (3.3)$$

This supplies the friction and windage losses which can be assumed constant, and the no-load stray loss which can be taken as the loss due to high frequency tooth ripple in the main flux, and in the zigzag leakage flux produced by the magnetizing current. Although  $R_2$  is not

known accurately, especially in the squirrel-cage machines, a scale is fixed for the quantity  $msV_1^2$  in terms of power by plotting both the product  $sV_1^2$  and the input power against voltage, and extrapolating to zero voltage when the two quantities must be equal. In this test performed, it was always found that  $sV_1^2$  increased with increasing  $V_1$ . Ignoring for a moment the hysteresis torque, it follows that

$$\frac{\text{change in } sV_1^2 \text{ from zero to full voltage}}{\text{values of } sV_1^2 \text{ at zero voltage}} = \frac{\text{harmonic losses}}{\text{friction and windage losses}}$$

The left-hand ratio is determined from the curve of  $sV_1^2$ , and the friction and windage losses are determined from the usual no-load power versus voltage curve, extrapolated to zero. The latter curve, in fact, is used to put a scale on the  $sV_1^2$  versus voltage curve. Thus harmonic losses are obtained. There is also an additional transference of power to the rotor by the hysteretic action of the primary field on the secondary. The power transferred synchronously in this manner is equal to the hysteresis loss which would have occurred in the same secondary iron, at the same flux density, at fundamental frequency. In order to apply the small correction for  $I^2R$  losses in the primary copper it is necessary to measure the currents throughout. The test routine, therefore, is to measure simultaneous values of power, current and slip for a series of voltages. Thus

the values needed for the  $sv^2$  versus voltage curve, the power versus voltage curve, and the  $I^2R$  correction, are obtained. The power versus voltage curve also gives the sum of the total fundamental primary iron-loss and harmonic losses, and, since the latter are determined in this test, the former follows by difference. Figure 3.2 demonstrates a typical  $sv_1^2$  versus voltage curve.

#### 3.4.2 The Reverse Rotation Test

The reverse rotation test was proposed by Morgan, Brown and Schumer [11] and remains the preferred method for measuring high frequency pulsation losses according to the I.E.E.E. test code. The stray loss due to the leakage flux of magnetizing current can be obtained from this test. It gives the total loss due to the corresponding currents in both primary and secondary winding. Barton and Ahmad [14] suggest that, because of the experimental evidence the zigzag leakage flux component of the loss is approximately proportional to  $(\text{speed})^{1.6}$  and  $(\text{current})^{1.9}$ , the results of reverse rotation test extrapolated according to this law are sufficient, together with no-load stray loss obtained from Rawcliffe and Menon test to predict the total stray losses over the whole practicable speed range.

The reverse rotation test is carried out by applying reduced balanced polyphase voltage to the stator terminals



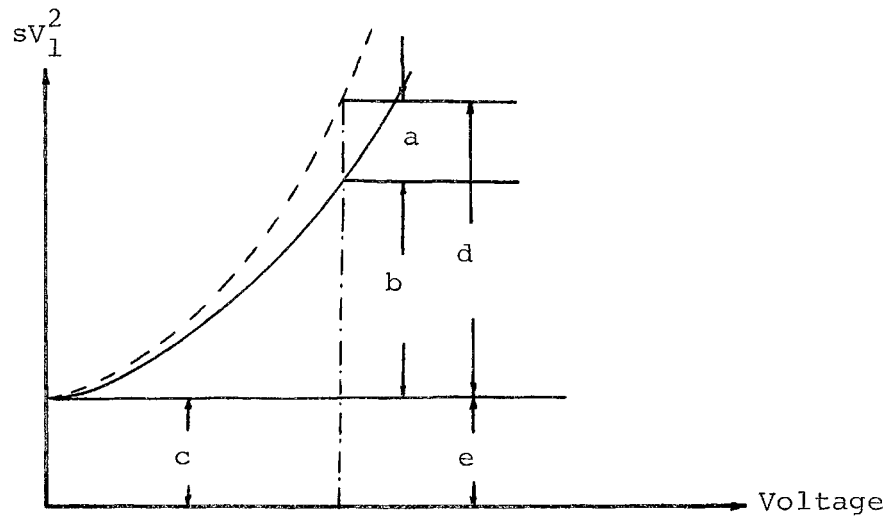


Figure 3.2 Typical  $sV_1^2$ /Voltage Curves

- (a) proportional to hysteresis loss
- (b) total change in  $sV_1^2$
- (c)  $sV_1^2$  at zero voltage (This value of  $sV_1^2$  is equivalent  
(in watts) to the friction loss  
as derived from power/voltage  
curve.)
- (d) proportional to total stray loss at no-load
- (e) proportional to friction and windage losses

—  $sV_1^2$  curve

---- corrected (hysteresis loss included)  $sV_1^2$  curve.

of the machine being investigated while driving the rotor at synchronous speed in the direction opposite to that of the revolving stator field. The stator current may be set at any desired value by adjustment of the applied voltage. Two power measurements are necessary: the power required to drive the rotor and the power input to the stator circuit. The former may be designated  $P_r$  and the latter  $W_s$ . The friction and windage losses at synchronous speed of the motor under test are also required and may be designated by  $P_m$ . The difference between these two quantities gives the component of the net input to the rotor which is supplied through the driving mechanical power. If this net power resulting from rotation be represented by  $P$ , then:

$$P = P_r - P_m \quad (3.4)$$

The net stator power,  $W$ , may be obtained by subtracting the stator copper loss from the stator input:

$$W = W_s - I^2 R \text{ stator loss} \quad (3.5)$$

The value of stray load loss is then obtained as the difference between net stator input and net stator power, or

$$\text{Stray load loss} = P - W \quad (3.6)$$

The reverse rotation test gives a measurement of all tooth frequency components. The test procedure assumes that the direction of rotation of the rotor with respect to the direction of the fundamental flux does not alter the magnitude of the tooth frequency losses, since in both cases the tooth frequency fluxes are superimposed upon fundamental frequency fluxes.

When the rotor of the machine is turned at synchronous speed in the direction opposite to the field flux all power supplied is consumed in losses. The total power input consists of electric power through the stator and mechanical power supplied through rotation. After subtracting stator copper losses and friction and windage losses from the total power input the remaining losses may be classified in three frequency categories:

- (1) fundamental frequency losses due to the leakage flux of the stator
- (2) double frequency losses in the rotor resulting from reverse rotation, and
- (3) tooth frequency components of the stray loss occurring in both rotor and stator.

This test neglects the fundamental frequency loss and includes it only through compensating effects. It is assumed that double frequency rotor losses are supplied in equal amounts from P and W. The tooth frequency losses result directly from rotation, and consequently are supplied only by mechanical power. Thus the net power

input through rotation P consists of one-half the double frequency rotor losses and the total tooth frequency losses. By subtracting from this quantity P the air-gap power supplied from the stator W, the tooth frequency losses are separated out and given as the remainder.

The question may be raised regarding the amount of the error introduced by neglecting the component of the stray loss which might be assumed to exist because of the fundamental frequency leakage flux. As a matter of fact, the proposed treatment not only neglects this component of the loss but includes it in the stator value W which is subtracted from the net rotational power input component P, thus doubling this error.

#### 3.4.3 The Ware's Test

A paper [18] by Ware established a test to measure the fundamental frequency component of stray loss. This test consists in applying reduced polyphase voltage to the stator with the rotor removed. Measurements of input power  $W_s$  and stator copper loss under these conditions yields to

$$LL_s = W_s - \text{Stator } I^2R\text{-loss} \quad (3.7)$$

where

$LL_s$  = fundamental frequency stray load loss.

This results in the existing test code procedure which is:

$$P_{st} = LL_s + LL_r \quad (3.8)$$

where

$LL_r$  = high frequency stray load loss

The higher frequency losses have the fundamental frequency component deducted during calculation. Thus:

$$LL_r = (P_r - P_m) - (W_r - LL_s - \text{Stator } I^2R\text{-loss}) \quad (3.9)$$

### 3.5 Practical Application of Test Procedures

There are three tests to be performed, the no-load, the standstill, and the reverse rotation tests.

#### 3.5.1 Reverse Rotation Test

The test code recommendations of currents to be used during this test were closely followed. They require the test current to be

$$I_r = \sqrt{I_1^2 - I_{NL}^2} \quad (3.10)$$

where

$I_r$  = value of stator current during reverse rotation test

$I_1$  = stator current, and

$I_{NL}$  = no-load current

For each value of test-current used during the reverse rotation test, readings of input voltage, current, and power were measured from carefully zeroed meters.

Output torque was carefully read from the torque transducer output. Values taken both with and without stator applied voltage yielded rotational power,  $P_r$ , and friction and windage power,  $P_m$ . Winding temperature readings were taken from embedded thermocouples and the stator resistance was corrected to correspond to the temperature at the test. The equation (3.6) gives the stray load losses from the data of the test results.

It is evident from equation (3.10) that the no-load stray losses cannot be determined from the reverse rotation test.

The no-load stray losses are the sum of the stray loss at fundamental frequency and the loss due to the high-order flux harmonics. The above losses can be determined either from standstill and no-load tests or from Rawcliffe and Menon test. The Rawcliffe and Menon test as described in Section 3.4.1 is essentially a graphical method derived from the no-load test, which was not considered, as, firstly an independent practical test, and secondly as accurate as the no-load test, because of the graphical extrapolation.

A third alternative is the test by Ware [18] which proposed the measurement of the fundamental frequency component of the stray losses by applying reduced polyphase voltage to the stator. Since this test requires the removal of the rotor, it was considered as an

impractical procedure. Therefore the standstill, and no-load tests were performed to determine stray losses associated with the fundamental and higher frequencies.

### 3.5.2 No-Load and Standstill Tests

The no-load test was performed according to Section 2.2.4. The no-load power curves were obtained for a full range of applied voltages. Values of friction and windage losses were obtained. By subtracting this from the total no-load loss at rated voltage, the value of the fundamental primary iron loss plus the total harmonic losses was determined. The correction for  $I^2R$ -loss in the primary copper was made. Finally, the standstill power input with open circuited secondary at rated voltage was measured. Thus the following were known:

- (1) (Stator fundamental iron-loss) + (total harmonic loss)
- (2) (Stator fundamental iron-loss).

Hence the two quantities were deduced from the expressions.

Table 3.2 gives the summary of the test results.

### 3.6 Determination of Stray Losses Due to the Harmonics

Since the most common part of the induction machine stray load losses is that produced by the air-gap harmonic fluxes which cross the air-gap and induce currents in the iron and/or in the copper on the other side, it was attempted to determine the stray load losses due to the

harmonics in the air-gap flux by calculating the harmonic e.m.f.'s of the stator winding and then the higher harmonic losses due to them.

Three cases of running conditions are described in the following, which were considered also for determination of harmonic losses in the machine.

### 3.6.1 No-Load Condition

At no-load the slip is generally less than 0.01, and the rotor currents, then, have a very small frequency. The induced e.m.f. is very small. Therefore the majority of the flux produced is mutual. Figure 3.3 demonstrates the no-load condition.

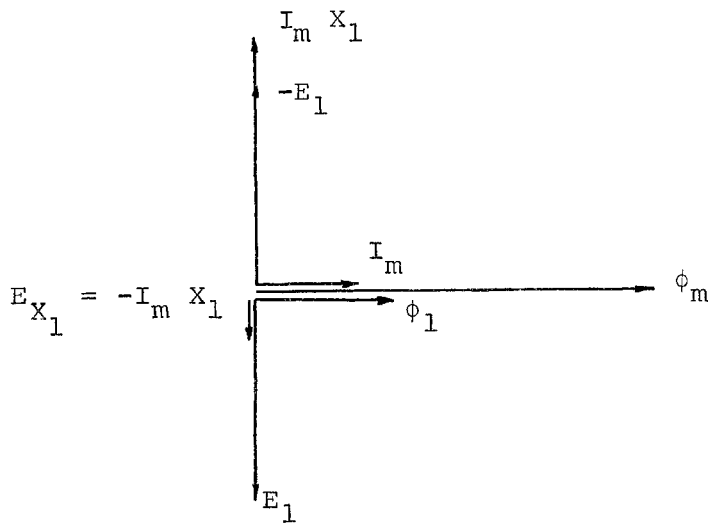


Figure 3.3 No-Load Condition



Some flux, however, denoted by  $\phi_1$ , does not link the rotor. This is a small portion, perhaps 2-3 percent of the total. The total stator flux is  $\phi_m + \phi_1$ , added arithmetically because there is no appreciable rotor current, but only the stator m.m.f. acting on the magnetic circuit. The stator current is the same as the magnetizing current  $I_m$ . The air-gap fluxes are responsible for the induction of  $E_1$  and  $E_{X_1} = -I_m X_1$ , to the sum of which the applied voltage  $V_1$  is equal and in phase opposition. This neglects the stator resistance drop, which is permissible.

### 3.6.2 Half-Load and Full-Load Conditions

Under any and every condition of load, the stator flux components  $\phi_m$  and  $\phi_1$  must sum vectorially to a total which will induce in each stator phase an e.m.f. equal to the applied voltage (neglecting resistance)[19]. Thus at full load, Figure 3.4, the mutual flux  $\phi_m$  has induced an e.m.f. in the rotor, which causes a current to circulate. The ampere-turns of the rotor tend to demagnetize the machine, so that the stator takes an equal and opposite ampere-turn component, which in turn produces a greater stator leakage flux  $\phi_1$ . Thus  $\phi_m$  must be reduced.

The reduction is not equal to the increase of  $\phi_1$ , because  $\phi_1$  is produced by the stator current alone, while  $\phi_m$  results from the combination of both stator and

rotor ampere-turns, and is due to their resultant.  $\phi_m$  does, nevertheless, fall appreciably, and it is considered to be constant within the load range to be investigated.

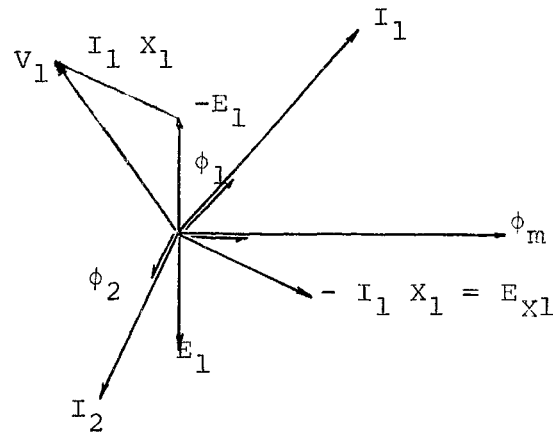


Figure 3.4 Half-Load and Full-Load Conditions

### 3.7 Practical Application of the Test Procedure

The rotor of the induction machine under test was short circuited and the stator excited with the rated voltage. The air-gap flux was recorded on a magnetic tape for no-load, half-load and full-load cases. These experimental data were sampled using the IBM 1827 A/D converter in conjunction with the IBM 370 digital computer. In selecting the sampling interval, the main consideration was to satisfy the sampling theorem. The sampling rate was adjusted to 80 samples per period. A total record length of 5.1 sec was digitized in each

case.

In order to determine the harmonic contents of the air-gap flux, the discrete Fourier series with piecewise approximation as described in Appendix II was used. The advantage of this method as compared to the Fast Fourier transform is its independency of the equal time increment. In order to verify this the following two steps were carried out:

(a) The Fast Fourier transform was used for determination of the harmonics by taking sufficient samples per period. The result of the harmonic analysis obtained agree with those of the discrete Fourier series.

(b) It was attempted to reproduce the actual waveform of the air-gap flux using the piecewise approximation. The frequency spectra, the actual air-gap flux at no-load and full-load and its Fourier approximation are plotted at the end of this chapter.

In Figures 3.8(a) and 3.9 (b) the points denote the curve of the actual air-gap flux and the lined curve demonstrates its Fourier approximation. The discrepancies at some minima and maxima are due to the higher pulsations at these points, which were not entered in the Fourier generating function.

### 3.7.1 The Analysis of Harmonic Losses at No-Load

The stator search coil which is mounted between the

slots 1 and 7 of the stator winding in the machine under test allows the measurement of induced voltage in this coil. This induced voltage is proportional to the main flux  $\phi_m$  in the air-gap. Hence the harmonic contents in the air-gap flux can be determined as described in Section 3.7. The harmonic r.m.s. phase e.m.f.'s in the stator winding are calculated according to [19] as follows:

$$E_n = E_1 \frac{Kd_n \cdot Ke_n}{Kd_1 \cdot Ke_1} \cdot \frac{B_n}{B_1} \quad (3.11)$$

where

$E_1$  = r.m.s. phase e.m.f. at fundamental frequency

$Kd_1$  = distribution factor at fundamental frequency

$$= \frac{\sin \frac{1}{2} \sigma}{g' \sin (\sigma/g')} \quad (3.12)$$

$\sigma = 60^\circ$  = the phase spread

$g' = 3$  slots per pole per phase

$Kd_n$  = distribution factor of harmonics

$$= \frac{\sin \frac{1}{2} n \sigma}{g' \sin \frac{1}{2} (n \sigma / g')} \quad (3.13)$$

$n$  = order of harmonics

$Ke_1$  = coil-span factor at fundamental frequency

$$= \frac{1}{2} \epsilon \quad (3.14)$$

$\epsilon = \frac{2}{9} \pi$  = the angle by which the span departs from  
its full pitch value  $\pi$

$$K e_n = \cos \frac{1}{2} n \epsilon \quad (3.15)$$

$\frac{B_n}{B_1}$  = ratio of harmonics flux density

Calculating  $E_1$  from equivalent circuit 2.3(a) under each load condition the harmonic r.m.s. phase e.m.f.'s can be determined from equation (3.11). In order to be able to use the relation (3.11) two assumptions are to be made:

(a) The r.m.s. phase e.m.f. of stator winding will be

$$E = \sqrt{(E_1^2 + E_3^2 + \dots + E_n^2)} \quad (3.16)$$

Because of small values of harmonic e.m.f.'s as compared with the fundamental e.m.f.  $E_1$ , this,  $E$ , is indistinguishable from  $E_1$ .

(b) The fundamental flux component  $\phi_1$  differs slightly from the total flux  $\phi_m$  per pole, so that the equation (3.11) with  $B_1 \sim \phi_1$  instead of  $B_m \sim \phi_m$  causes very little inaccuracy.

Now the energy of the magnetic field stored in the air-gap due to the harmonics is given as

$$W = \sum_{n=1}^{\infty} \frac{q}{2} \cdot I_{m_n} \cdot E_n \cdot \cos \alpha \quad (3.17)$$

where

$q$  = number of phases, in this case  $q = 3$ ,

$I_m$  = the magnetizing current which at no-load is equal to the stator current, neglecting a very small portion of the rotor current, since the slip at no-load in the machine under test equals 0.005.

$E_n$  = the harmonic e.m.f.'s, and

$\alpha$  = the angle between each harmonic e.m.f.  $E_n$  and the magnetizing current.

It was assumed that the fundamental e.m.f. and the harmonic e.m.f.'s are in the same direction and they have the same phase angle against the magnetizing current.

An analysis for the determination of the different phase angle  $\alpha$ 's showed that at no-load in the case of the fundamental e.m.f.,  $E_1$ ,  $\alpha = 87^\circ$  and in the case of most significant harmonic e.m.f.,  $E_{17}$ ,  $\alpha = 86^\circ$ . Similar results were obtained for half-load and full-load. Therefore all e.m.f.'s were considered to lie in the same direction. The results of the different tests for determination of the stray load losses are given in Table 3.2.

| $P_{st}$   | Watts |
|--|-------|
| Rawcliffe and Menon test   | 30    |
| No-load and Standstill test  | 32    |
| Harmonic Analysis  | 14.6  |
| $H\left(\frac{n_o}{n_s}\right)^{1.6} \left(\frac{I_l}{I_r}\right)^{1.9}$ | 16    |

Table 3.2 Test Data at No-load from  
Various Methods

The reverse rotation test measures all losses associated with the zigzag leakage flux, but this test cannot be performed at no-load, because of the equation (3.10).

Since the stray loss due to the leakage flux is proportional to the (current)<sup>1.9</sup>, at small slips, including the no-load slip, it can be calculated accurately by the means of extrapolation, i.e. using the equation (3.1). In Table 3.2 the combination of the results obtained from reverse rotation test and the equation (3.1) comprise the total stray load losses.

### 3.7.2 Stray Losses at Half-Load and Full-Load

From reverse rotation test the stray losses at half-load and full-load were determined, using the following formula

$$P_{st} = H \left( \frac{n_o}{n_s} \right)^{1.6} \left( \frac{I_l}{I_r} \right)^{1.9} \quad (3.18)$$

Where  $H$ ,  $n_s$  and  $I_r$  are given in Table 3.2 and Appendix I, as the result of a test investigated by Barton and Ahmad [14], the results of the reverse rotation test were extrapolated according to this law.

### 3.7.3 The Analysis of Harmonic Losses at Half-Load and Full-Load

The procedure is the same as in the case of no-load. The magnetizing current  $I_m$ , as the difference of stator and rotor current, is the net current available for producing the air-gap field  $\phi_m$ . The summaries of different tests for the determination of stray losses at half-load and full-load are given in Tables 3.3 and 3.4.

| $P_{st}$  | Watts |
|---|-------|
| Reverse rotation test   | 31    |
| $H \left( \frac{n_o}{n_s} \right)^{1.6} \left( \frac{I_l}{I_r} \right)^{1.9}$ | 32.4  |
| Harmonic Analysis   | 16.23 |

Table 3.3 Test Data at Half-Load from  
Various Methods



Using equation (3.18) the calculated torque-slip curves were plotted with and without the effect of the stray losses. Figure 3.6 demonstrates these curves.

| $P_{st}$  | Watts |
|---|-------|
| Reverse rotation test   | 35.46 |
| $H \left( \frac{n_o}{n_s} \right)^{1.6} \left( \frac{I_l}{I_r} \right)^{1.9}$ | 45.56 |
| Harmonic Analysis   | 18.30 |

Table 3.4 Test Data at Full-Load from  
Various Methods

At no-load the stray losses can be considered as the sum of the losses due to the high frequency tooth ripple in the main flux and zigzag leakage flux produced by the magnetizing current. The harmonic losses obtained from the air-gap flux in the machine under test are associated with the tooth ripple in the main flux, since only the main flux of the magnetizing current could be measured through the stator search coil. These losses compose of 45 percent of the total stray load losses.

The reverse rotation test measures at half-load and full-load the stray losses associated with the zigzag leakage flux of the magnetizing current. On the other

hand the harmonic losses calculated through the air-gap flux, in both cases, are due to the main flux. Therefore adding to the results of the reverse rotation test, in both cases, the amount of the loss associated with the main flux produced by the magnetizing current, then the obtained results from the air-gap harmonics will compose nearly 30 percent of the total stray load losses. Figure 3.5 shows the torque-slip curve with and without the stray load losses and Table 3.5 demonstrates the different components and the suggested methods for measuring or calculating these. Since harmonic losses as a part of the total stray load losses under each load condition depend upon the harmonics content in the air-gap flux, it is evident that the design aspects of the stator and rotor circuits determine these harmonics and the corresponding losses. Hence it was attempted to investigate the stator and rotor circuits and the effect of the field harmonics of the induction machine under test in the following.

### 3.8 Some Aspects of Harmonic Analysis

The air-gap flux of the machine under test was measured through a search coil which was mounted between the slots 1 and 7 of stator winding. The current in the rotor circuit was measured and a reverse test was performed in which the rotor was excited and the stator

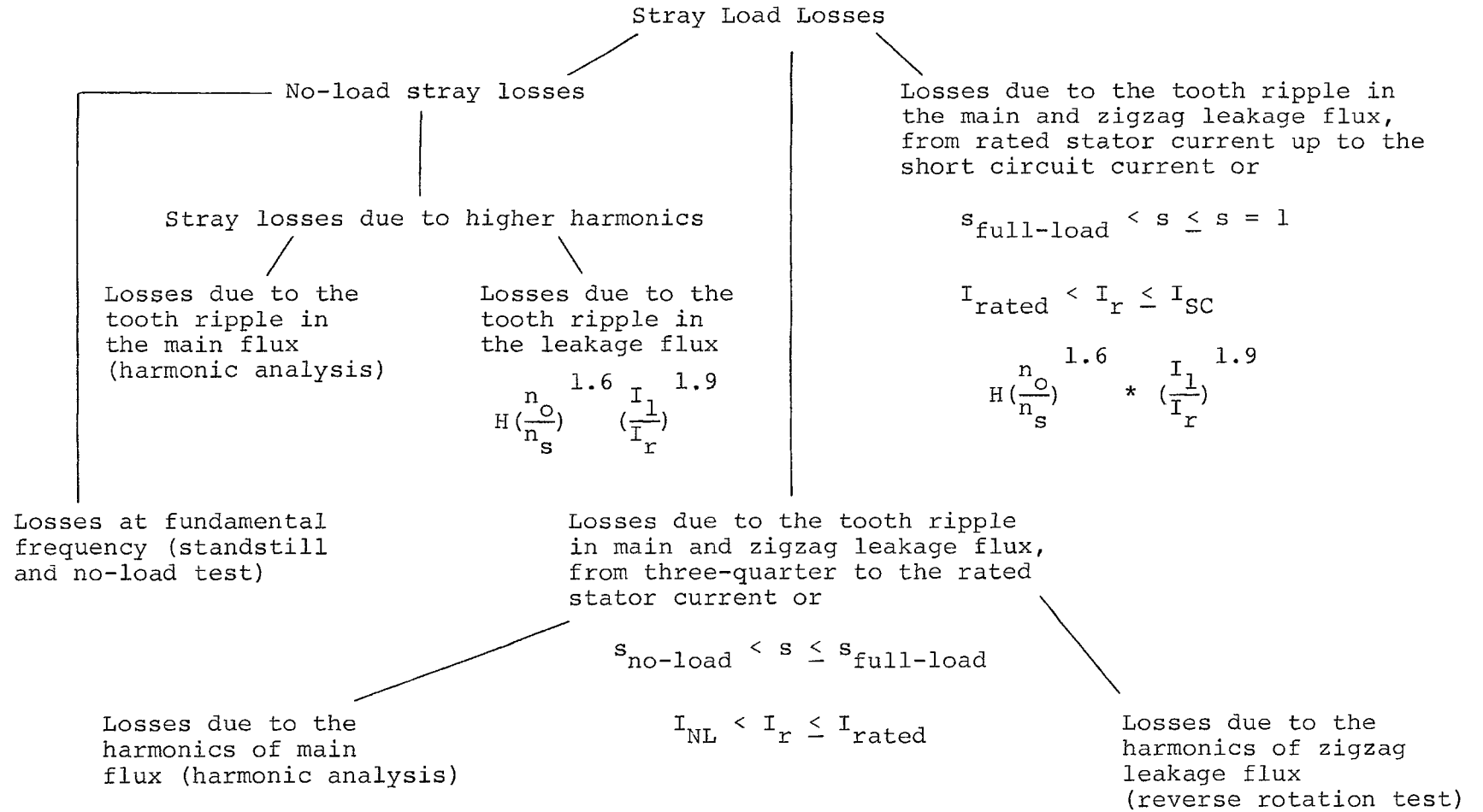


Table 3.5 Components of Stray Losses and Suggested Measurements

current measured. These tests were performed for three running conditions, no-load, half-load and full-load. The rotor was fed with a voltage which gave, as nearly as possible, the same flux condition in the machine as does the rated voltage applied to the stator. It is not possible to meet this condition exactly, for with the stator as primary, the stator flux will exceed the rotor flux, and vice versa with the rotor as primary. It can, however, be arranged that the main flux condition in the machine is the same in the two cases.

Therefore the value of the rotor voltage was obtained from the test for the determination of the Blondel coefficient  $\sigma$  in Section 4.4.1. The analysis of the harmonics content in the air-gap flux, rotor and stator current for the three running conditions shows the following characteristics:

The triplen harmonics appeared in all three cases, though the machine is star connected, and hence all triplen harmonics should be suppressed. The 5th, 7th, 11th and 15th harmonics were significant and they were produced in the stator circuit.

The distribution factors for harmonics are given as

$$n = 6Ag' \pm x,$$

where  $n$  is the order of the harmonic,  $A$  any integer 0,1,2, ..., and  $x$  any odd number. Thus for  $g' = 3$  stator slots

per pole per phase,  $A = 1$ , and  $x = 1$ , the 17th and 19th harmonics were produced in the stator circuit strongly. On the rotor with  $g' = 2$  rotor slots per pole per phase, the 13th, 23rd, and 25th harmonics are established significantly.

Following the results obtained from harmonic analysis, the amount of stray loss due to the harmonics could be reduced largely by making the stator and rotor slot pitches near equal, but attention should be paid to the rotor locking and crawling effects. However this amount can be minimized by having the two pitches as nearly equal as possible by using the least possible number of slots per pole per phase. The contribution of 17th harmonic to the total higher harmonic losses at no-load is about 18.8 percent, which could be eliminated by having  $g'$ , as the number of slots per pole per phase, equal 2 instead of 3 in the machine under test. On the other hand the equality of stator and rotor slots may tend to the effect of cogging, by which the machine may refuse to start at all. But in the case of a higher starting torque in the slip-ring machines the latter phenomenon is less prominent.

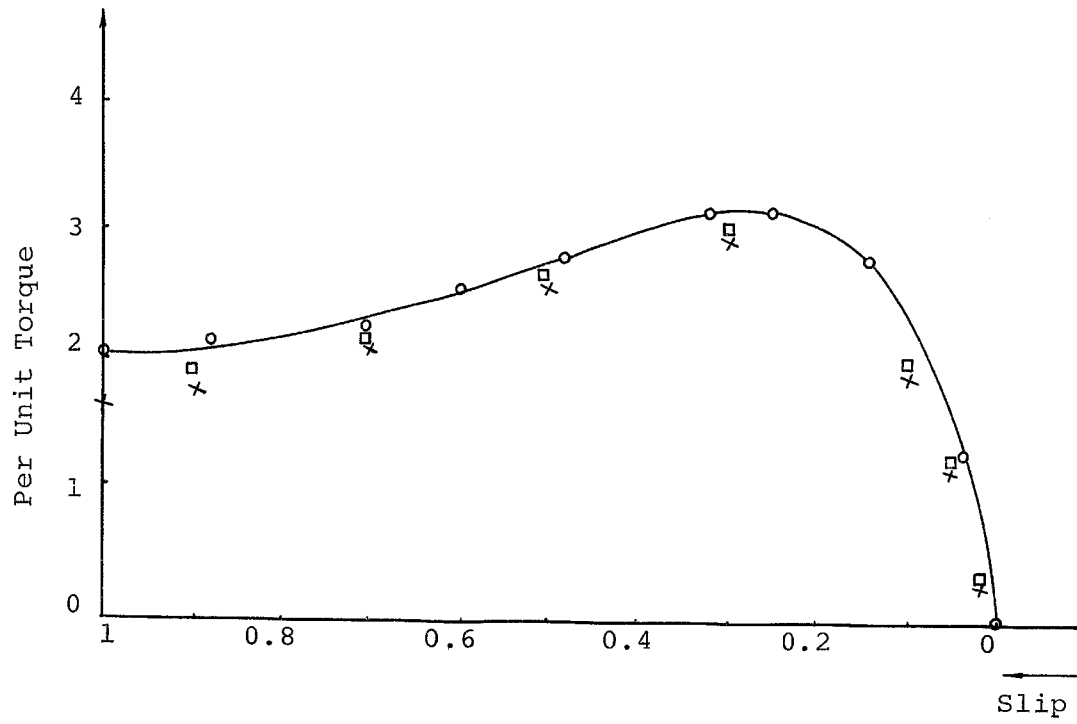


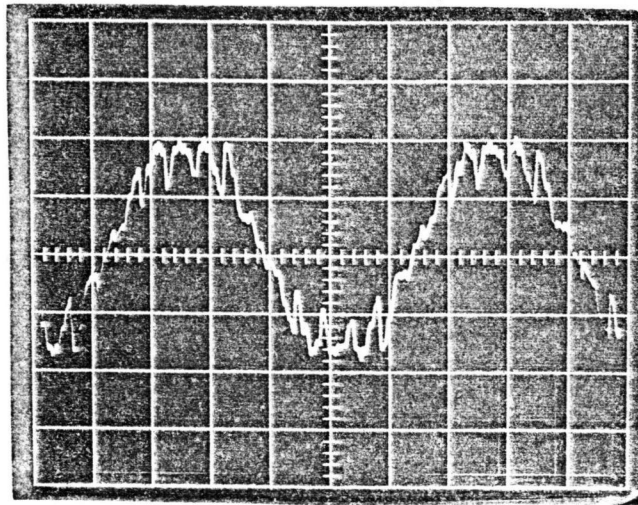
Figure 3.5 Per Unit Torque versus Slip

○ — ○ — ○ measured

+ + + I.E.E.E. Test Code without Stray Losses

□ □ □ I.E.E.E. Test Code with Stray Losses

Base Torque = 15 ft-lb.



Scale: 0.2 V/div

0.2 sec/div

Scale: 2V/cm

paper speed 40 mm/sec

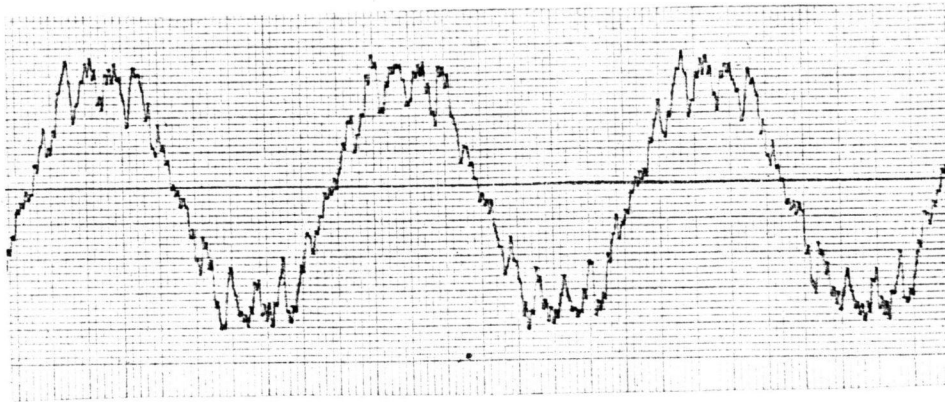
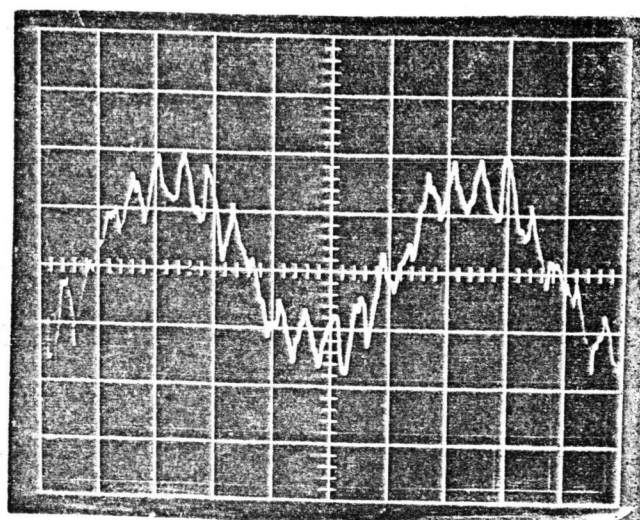


Figure 3.6 Air-Gap Flux at No-Load



Scale: 2V/div

0.2 sec/div

Scale: 2V/cm

paper speed 40 mm/sec

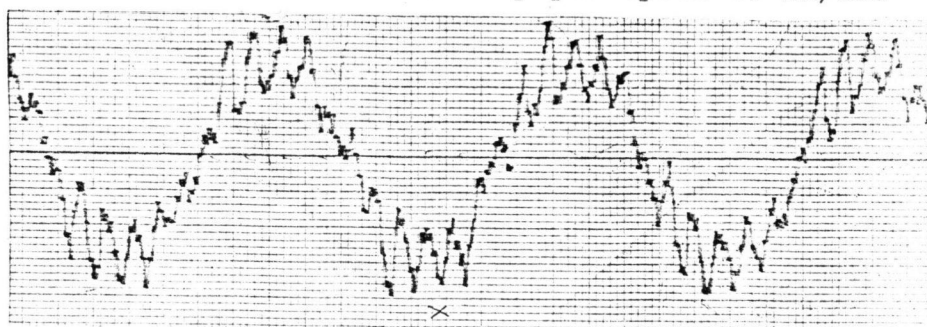


Figure 3.7 Air-Gap Flux at Full-Load



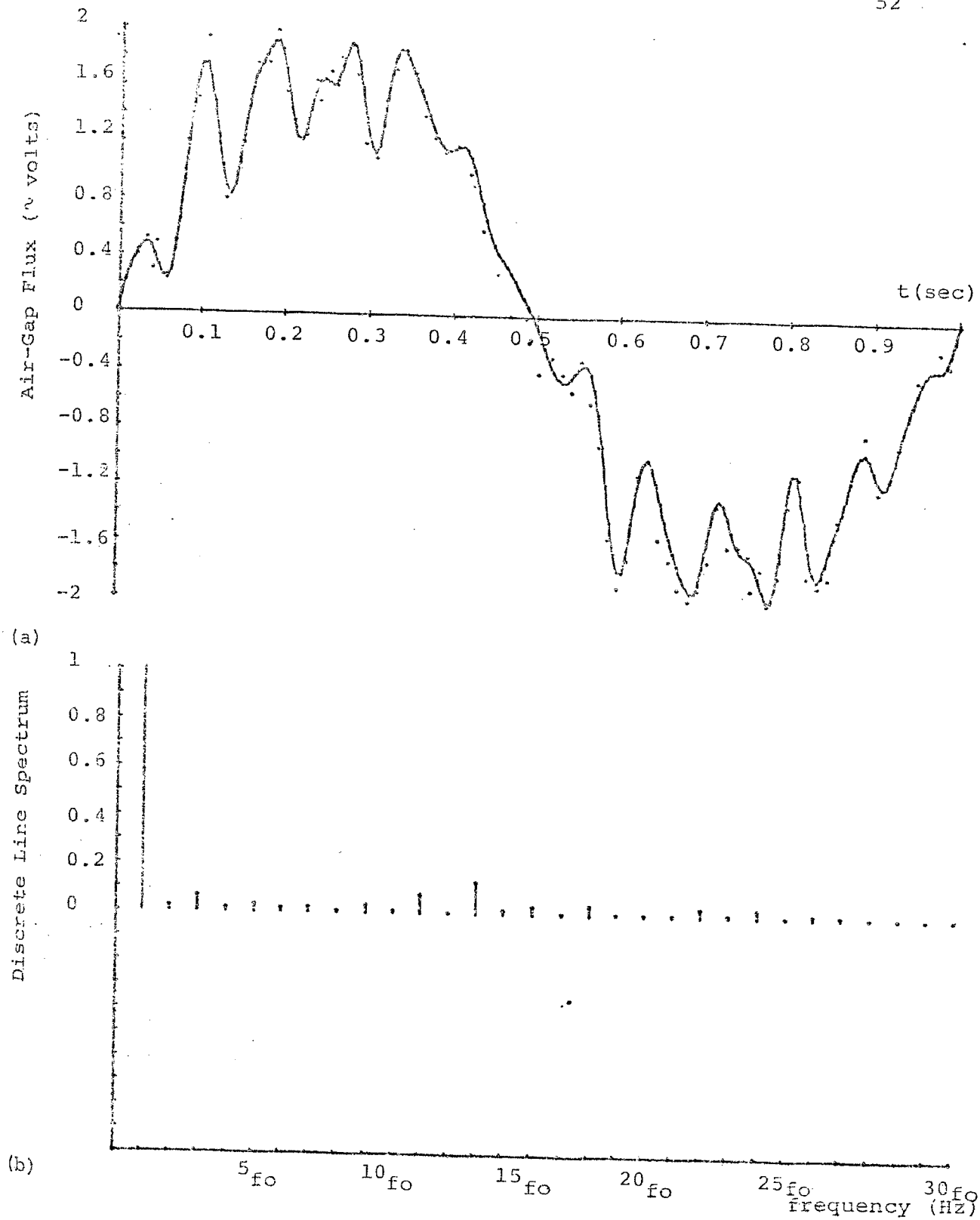


Figure 3.8 Air-gap Flux and Discrete Line Spectrum at No-Load

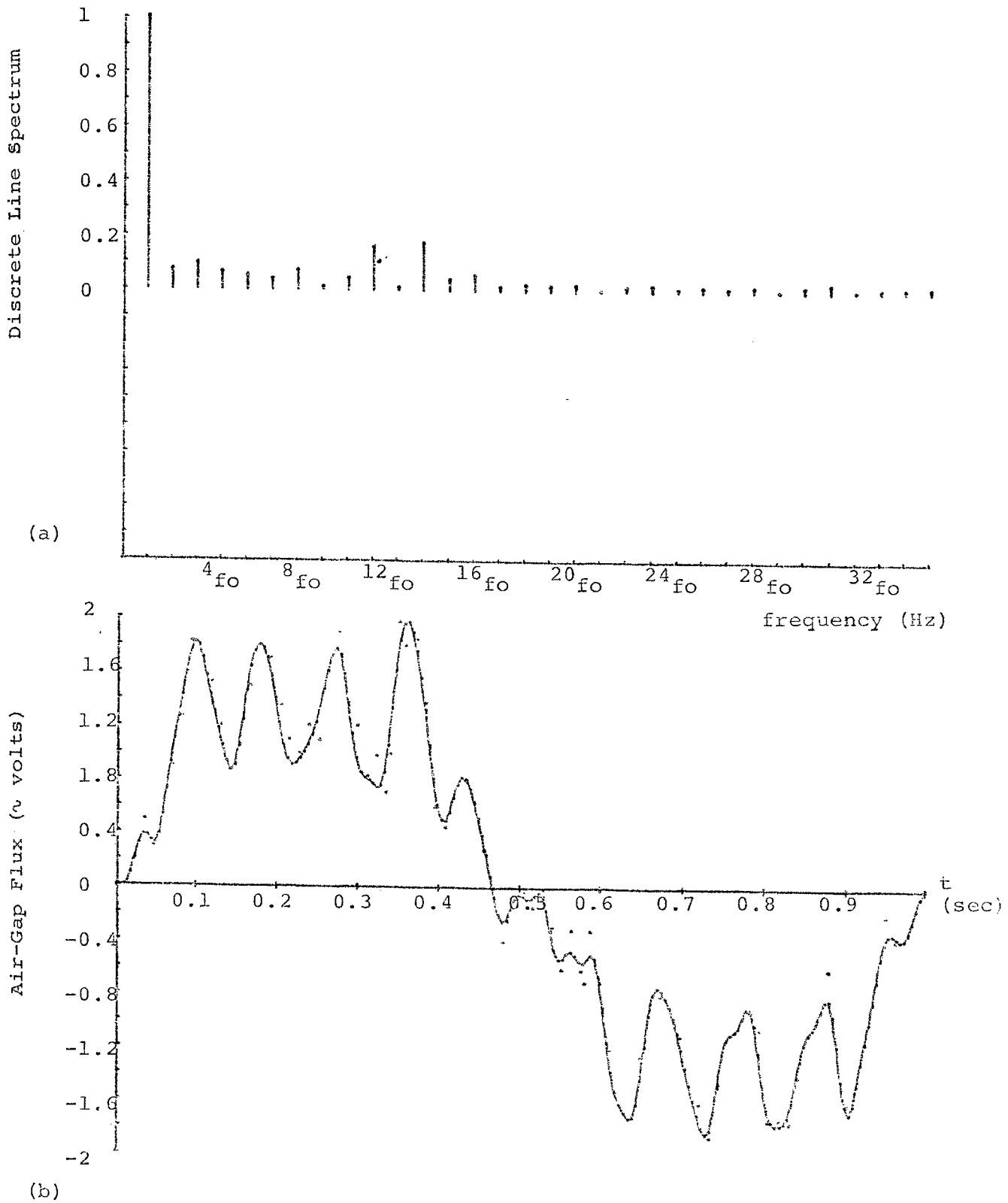


Figure 3.9 Discrete Line Spectrum and Air-Gap Flux  
at Full-Load.

## CHAPTER 4

### THE "EXACT" CIRCLE DIAGRAM OF THE INDUCTION MOTORS

#### 4.1 Introduction

The circle diagram of the induction machine appears to be an effective instrument to determine the machine performance. In this chapter two methods for drawing the circle diagram and determining the machine performance are discussed. By the first method [20] a general analytical proof of the "exact" circle diagram of the induction machine under test is introduced, using a complex notation and polar coordinates. The second method is likewise a graphical construction using the properties of inversion.

#### 4.2 The First Method of Constructing the "Exact" Circle Diagram

##### 4.2.1 Theory

The equivalent circuit of the induction motor is shown in Figure 4.1. It is assumed that the air-gap m.m.f. is proportional to the magnetizing current  $I_m$ , i.e. the effect of saturation is neglected.

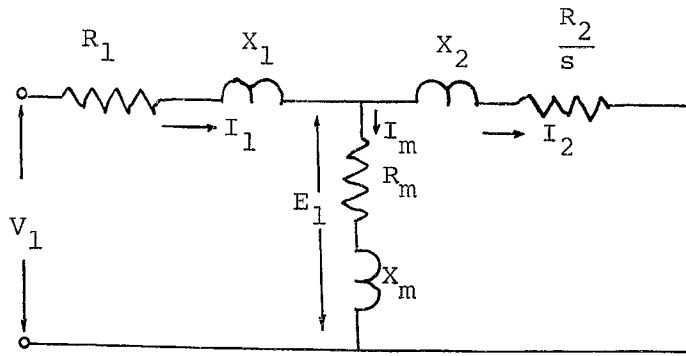


Figure 4.1 Equivalent Circuit of the Induction Motor

At no-load, the slip  $s$  can be taken as zero. Then the secondary impedance becomes infinite, and the no-load current is

$$I_{NL} = \frac{V_1}{R_1 + jX_1 + R_m + jX_m} = \frac{V_1}{Z_1 + Z_m} \quad (4.1)$$

The air-gap e.m.f. at no-load is

$$\begin{aligned} E_{NL} &= V_1 - I_{NL}(R_1 + jX_1) \\ &= V_1 \left( 1 - \frac{Z_1}{Z_1 + Z_m} \right) \end{aligned} \quad (4.2)$$

$$E_{NL} = V_1 \left( \frac{Z_m}{Z_1 + Z_m} \right) \quad (4.3)$$

In order to obtain an expression for the secondary equivalent current, Thevenin's Theorem is used, by which the circuit of Figure 4.1 is replaced by an e.m.f. source of  $E_{NL}$  with an internal impedance of  $Z_e$  applied to the secondary circuit of  $(R_2/s) + jX_2$  as shown in Figure 4.2 in which  $Z_e = (Z_1 Z_m)/(Z_1 + Z_m)$ .

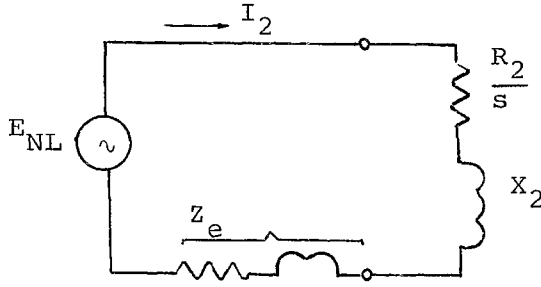


Figure 4.2

$$\begin{aligned}
 \text{Then } I_2 &= \frac{E_{NL}}{Z_e + \left(\frac{R_2}{s}\right) + jX_2} \\
 &= \frac{V(Z_m/(Z_1 + Z_m))}{(Z_1 Z_m)/(Z_1 + Z_m) + (R_2/s) + jX_2} \quad (4.4)
 \end{aligned}$$

Now one can set  $(Z_m/(Z_1 + Z_m)) = K$ , where  $K$  is a complex constant; hence

$$I_2 = \frac{KV_1}{KZ_1 + (R_2/s) + jX_2} \quad (4.5)$$

Consider now the air-gap and e.m.f.  $E_1$  when the primary current is  $I_1$ .

$$E_1 = V_1 - I_1 Z_1$$

The magnetizing current is then

$$I_m = E_1/Z_m = (V_1 - I_1 Z_1)/Z_m$$

Now  $I_1 = I_{NL} + I_{2A}$  by definition. Hence one obtains

$$\begin{aligned} I_m &= (V_1 - (I_{NL} + I_{2A})Z_1)/Z_m \\ &= \frac{1}{Z_m} (V_1 Z_m / (Z_1 + Z_m) - I_{2A} Z_1) \\ I_m &= I_{NL} - I_{2A} (Z_1/Z_m), \end{aligned} \quad (4.6)$$

and since  $I_1 = I_2 + I_m$ , and  $I_{2A} = I_1 - I_{NL}$ , therefore

$$\begin{aligned} I_{2A} &= I_2 - I_{2A} \frac{Z_1}{Z_m} \\ I_{2A} \left( \frac{Z_1 + Z_m}{Z_m} \right) &= \frac{K \cdot V_1}{KZ_1 + \frac{R_2}{s} + jX_2} \end{aligned}$$

or

$$\frac{I_{2A}}{K} = \frac{K \cdot V_1}{KZ_1 + \frac{R_2}{s} + jX_2}$$

i.e.

$$I_{2A} = \frac{K^2 V_1}{KZ_1 + \frac{R_2}{s} + jX_2} \quad (4.7)$$

It can readily be proven 22 that the locus of this current as  $s$  varies is part of a circle. Since  $I_1 = I_{NL} + I_{2A}$  and at zero slip the value of  $\frac{R_2}{s}$  is infinite so that  $I_{2A}$  is zero, it follows that the locus of  $I_1$  is part of a circle passing through the point  $I_1 = I_{NL}$ . Now the complex constant  $K$  can be calculated to a sufficient degree of accuracy as follows: By definition

$$K = |K| (\cos \alpha + j \sin \alpha) = \frac{Z_m}{Z_1 + Z_m}$$

Also from (4.3) one can calculate

$$K = \frac{E_{NL}}{V_1} = \left| \frac{E_{NL}}{V_1} \right| (\cos \alpha + j \sin \alpha)$$

Let  $I_\mu$  = numerical value of quadrature component of magnetizing current per phase at no-load  
calculated during desing

$W$  = iron loss per phase in watts.

One obtains from Figure 4.3 the vector diagram of the motor at no-load

$$I_{NL} = \left( \frac{W}{|E_{NL}|} - jI_\mu \right) (\cos \alpha + j \sin \alpha) \quad (4.8)$$

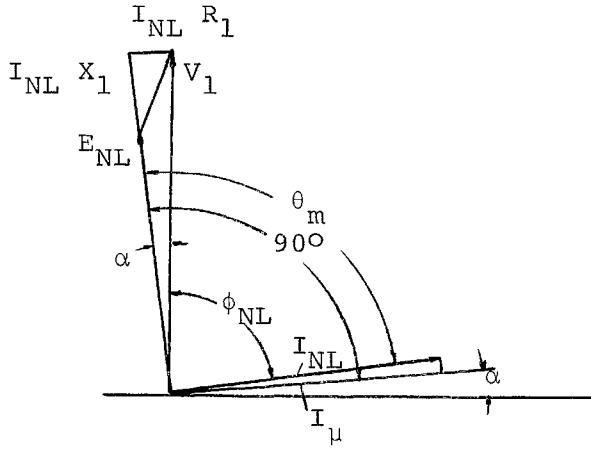


Figure 4.3 Vector Diagram at No-Load

Now  $E_{NL} \approx \sqrt{V_1^2 - (I_{\mu} R_1)^2} - I_{\mu} X_1$  and  $\alpha \approx \sin^{-1} \frac{I_{\mu} R_1}{V_1}$ , so that a close approximation to  $I_{NL}$  can be obtained by substitution in equation (4.8). Substituting this value of  $I_{NL}$  in equation (4.2) gives a more accurate value of  $E_{NL}$ . Then  $K = \frac{E_{NL}}{V_1}$  and  $Z_m = \frac{V_1}{I_{NL}} - (R_1 + jX_1)$ . Now let

$$Z_m = |Z_m| (\cos \theta_m + j \sin \theta_m)$$

where  $\theta_m = \tan^{-1} X_m/R_m$ . Substituting in equation (4.6) gives

$$I_m = I_{NL} - I_{2A} \frac{|Z_1|}{|Z_m|} [\cos (\theta_1 - \theta_m) + j \sin (\theta_1 - \theta_m)]$$

where

$$\theta_1 = \tan^{-1} \frac{X_1}{R_1},$$

or  $\sin \theta_m$  is normally greater than  $\theta_1$  one obtains

$$I_m = I_{NL} - I_{2A} \frac{|Z_1|}{|Z_m|} [\cos (\theta_m - \theta_1) - j \sin (\theta_m - \theta_1)] \quad (4.9)$$



Since  $I_{NL}$  is a constant vector and since the locus of  $I_{2A}$  is part of a circle, it follows that the locus of  $I_m$  is also part of a circle passing through the point  $I_m = I_{NL}$ .

In Figure 4.4 one can set  $OP$  equal to the primary current  $I_1$  and  $OA$  equal to the no-load current  $I_{NL}$ . Then  $AP$  represents  $I_{2A}$ . Now the vector  $AD$  is made equal in magnitude to  $(Z_1/Z_m) \cdot \overline{PA}$  and makes an angle  $(\theta_m - \theta_1)$  with  $PA$  produced, it follows from (4.9) that  $OD$  represents  $I_m$  in magnitude and phase.

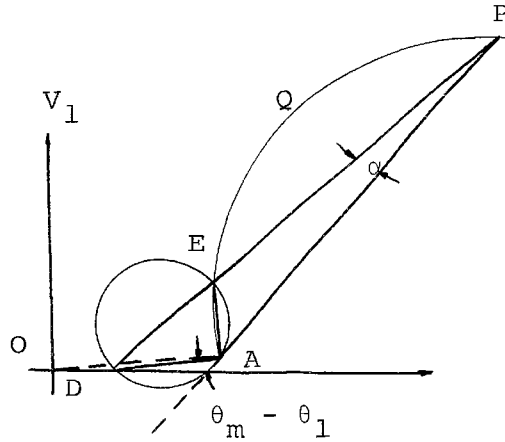


Figure 4.4

Now if  $AP$  represents  $I_{2A}$  then  $PA$  represents  $(-I_{2A})$  and

$$\overline{DP} = \left(\frac{1}{K}\right) \cdot \overline{AP}$$

From equations (4.5) and (4.7) one calculates

$$I_{2A} = K \cdot I_2$$

Hence DP represents  $I_2$  in magnitude and phase, and  $\angle DPA = \alpha$ .

Let the line DP intersect the arc AQP at E. Since the point P has been chosen arbitrarily, the angle EPA does not depend upon the position of P on the locus. It follows from the geometry of the Figure 4.4 that the point E on the locus must be a fixed point relative to the point A which is fixed, the line AE being a chord of the circle of which the locus AEQP is part.

It has been shown that the locus of  $I_m$  is a circle passing through the point  $I_m = I_{NL}$ , i.e., the locus of D as the position of the point P on its locus changes is a circle passing through the point A. Since the angle  $\angle ADE = (\theta_m - \theta_1) - \alpha$  is constant. The line joining the points A and E is a common chord to both circles which form the loci of  $I_1$  and  $I_m$ .

#### 4.2.2 Equivalent Simplified Circuit

Consider now equation (4.7)

$$I_{2A} = \frac{K^2 V_1}{KZ_1 + \frac{R_2}{s} + jX_2}$$

$$K^2 = |K|^2 (\cos 2\alpha + j \sin 2\alpha)$$

$$KZ_1 = |K| |Z_1| [\cos(\theta_1 + \alpha) + j \sin(\theta_1 + \alpha)],$$

where  $|K|$  is the modulus of K, and  $|Z_1|$  the modulus of  $Z_1$ .

Then

$$I_{2A} = \frac{|K|^2 V_1 (\cos 2\alpha + j \sin 2\alpha)}{|K| |Z_1| [\cos(\theta_1 + \alpha) + j \sin(\theta_1 + \alpha)] + \frac{R_2}{s} + jX_2}$$

with

$$r_1 = |K| |Z_1| \cos(\theta_1 + \alpha),$$

and

$$x_1 = |K| |Z_1| \sin(\theta_1 + \alpha)$$

Hence one obtains

$$I_{2A} = \frac{|K|^2 V_1 (\cos 2\alpha + j \sin 2\alpha)}{(r_1 + jx_1) + \frac{R_2}{s} + jX_2} \quad (4.10)$$

and

$$I_1 = I_{NL} + \frac{|K|^2 V_1 (\cos 2\alpha + j \sin 2\alpha)}{(r_1 + jx_1) + \frac{R_2}{s} + jX_2}$$

One can see that the primary current  $I_1$  is equivalent to a total current taken by the equivalent simplified circuit shown in Figure 4.5 in which the normal primary impedance of  $R_1 + jX_1$  is replaced by  $r_1 + jx_1$  and in which the applied voltage is equal to  $|K|^2 V_1$  in magnitude and is rotated in phase by angle of  $2\alpha$  in an anti-clockwise direction relative to  $V_1$ .

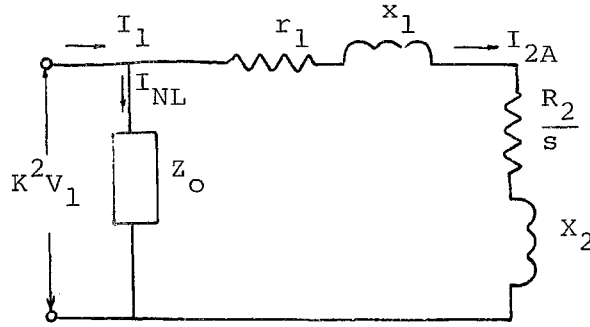


Figure 4.5 Equivalent Simplified Circuit

The value of the magnetizing impedance  $Z_O$  can be determined as follows

$$Z_O = \frac{K^2 V_1}{I_{NL}},$$

and substituting the  $I_{NL}$  from equation (4.1) gives

$$Z_O = K^2 (Z_1 + Z_m) = KZ_m \quad (4.11)$$

#### 4.2.3 Construction of Exact Circle Diagram from Design

##### Data

Figure 4.6 shows the circle diagram to be constructed. OA represents  $I_{NL}$  in magnitude and phase. We set  $s = \infty$  and make  $r_1$  equal to zero so that the equation (4.10) gives

$$I_{2A_i} = \frac{|K|^2 V_1}{j(x_1 + x_2)} (\cos 2\alpha + j \sin 2\alpha) \quad (4.12)$$

This equation demonstrates the ideal short circuit value of  $I_{2A}$  and is represented by AC in Figure 4.6. Its magnitude is  $|K|^2 V_1 / (x_1 + x_2)$  and makes an angle  $2\alpha$  with the horizontal as shown. The locus of the primary current  $I_1$  is then the semicircle AEPKC'C drawn on AC as diameter.

If the magnitude of the vector AB is equal to  $(\frac{Z_1}{Z_m}) * CA$  and making an angle  $(\theta_m - \theta_1)$  clockwise relative to the direction of CA, then AB is a diameter of the circular locus  $I_m$ . The line BC passes through the point E of the loci  $I_1$  and  $I_m$ , and represents the ideal short circuit value of  $I_2$ . By setting  $s = \infty$  and giving  $r_1$  its true value  $r_1 = |K| \cdot |Z_1| \cdot \cos(\theta_1 + \alpha)$  we obtain from the equation (4.10)

$$I_{2A_\infty} = \frac{|K|^2 \cdot V_1}{r_1 + j(x_1 + x_2)} (\cos 2\alpha + j \sin 2\alpha) \quad (4.13)$$

This line is represented by AC' in Figure 4.6. The point C' can be located easily by

$$CC' = \frac{r_1}{\sqrt{r_1^2 + (x_1 + x_2)^2}} * \overline{AC} \quad (4.14)$$

B'C' and OB' represent then the vectors  $I_2$  and  $I_m$  respectively corresponding to infinite slip.

Similarly by setting  $s = 1$  in equation (4.10) we obtain

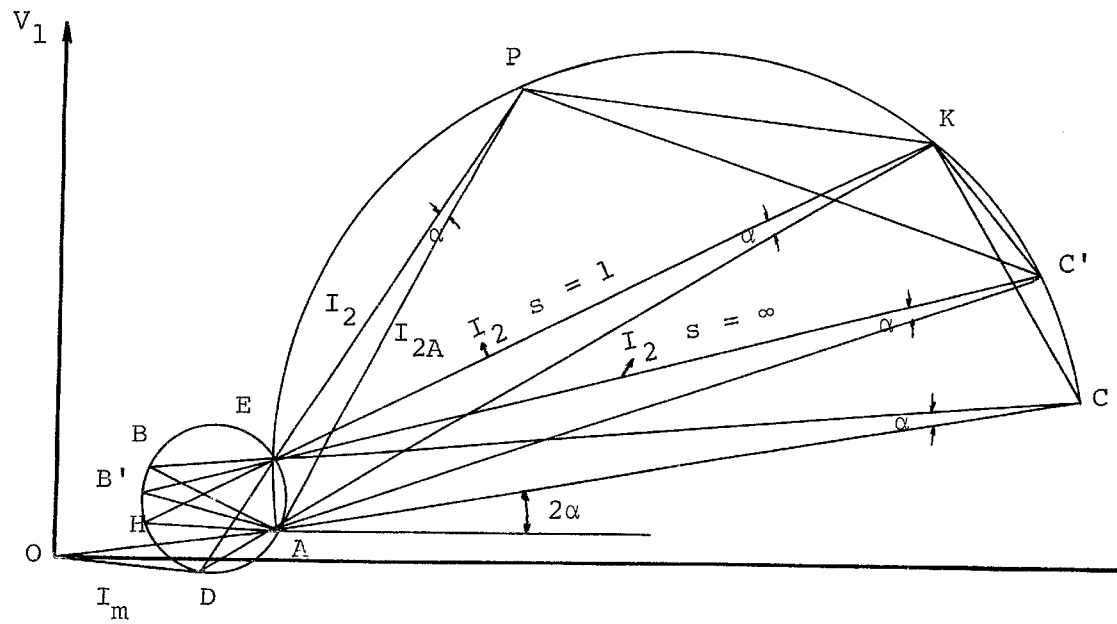


Figure 4.6 The Exact Circle Diagram of the Induction Motor

$$I_{2A_1} = \frac{|K|^2 V_1}{\sqrt{(r_1 + R_2)^2 + (x_1 + X_2)^2}} * \overline{AC} \quad (4.15)$$

Then HK and OH represent the short circuit values of  $I_2$  and  $I_m$  respectively. If P is any point on the locus of  $I_1$  corresponding to a value of slip  $s$  between  $s = 0$  and  $s = 1$ , then AP, DP and OD in Figure 4.6 represent the vectors  $I_{2A}$ ,  $I_2$  and  $I_m$  corresponding to this slip.

#### 4.2.4 Performance of the Motor

Although the circular locus of  $I_m$  in Figure 4.6 implies the usefulness of the exact circle diagram, it is not essential for the determination of the performance. This is illustrated in the following: In Figure 4.7, APKC'C is the semicircular locus of  $I_1$  and AU the drawn perpendicular to AC. Then AU represents the axis of  $K^2 V_1$ , being the applied voltage in the equivalent simplified circuit of Figure 4.5. Then AK and AC' represent the vectors  $I_{2A}$  corresponding to  $s = 1$  and  $s = \infty$ . With P as any point on the locus of  $I_1$  corresponding to a slip  $s$  between  $s = 0$  and  $s = 1$ , AP is the vector  $I_{2A}$  corresponding to this slip. Then the secondary equivalent current  $I_2$  is  $(\frac{1}{K}) * AP$ .

The line PS is drawn perpendicular to AC and intersecting AK and AC' at R and T. By similar triangles

$$\frac{RS}{AS} = \frac{CK}{AK} = \frac{r_1 + R_2}{x_1 + X_2}$$

Now

$$\begin{aligned} AS &= I_{2A} \cdot \sin \theta = I_{2A} \frac{x_1 + X_2}{\sqrt{\left(r_1 + \frac{R_2}{s}\right)^2 + (x_1 + X_2)^2}} \\ &= (I_{2A})^2 \cdot \frac{x_1 + X_2}{K^2 \cdot V_1} \end{aligned} \quad (4.16)$$

Thus

$$\begin{aligned} RS &= (I_{2A})^2 \frac{r_1 + R_2}{K^2 \cdot V_1} \\ RS \cdot V_1 &= I_2^2 (r_1 + R_2) \end{aligned} \quad (4.17)$$

$$\begin{aligned} PS &= I_{2A} \frac{r_1 + \frac{R_2}{s}}{\sqrt{\left(r_1 + \frac{R_2}{s}\right)^2 + (x_1 + X_2)^2}} \\ &= (I_{2A})^2 \frac{r_1 + \frac{R_2}{s}}{K^2 \cdot V_1} \end{aligned}$$

Thus

$$PS \cdot V_1 = I_2^2 \left(r_1 + \frac{R_2}{s}\right) \quad (4.18)$$

Subtracting (4.17) from (4.18) gives

$$PR \cdot V_1 = I_2^2 \cdot \frac{R_2}{s} (1 - s) \quad (4.19)$$



Equation (4.19) demonstrates the mechanical power.

By similar derivation one obtains

$$\begin{aligned} ST \cdot V_1 &= I_2^2 \cdot r_1 \\ PT \cdot V_1 &= I_2^2 \cdot \frac{R_2}{s} \end{aligned} \quad (4.20)$$

Equation (4.20) shows the developed torque in the machine.

The scale of slip can be constructed by drawing HA perpendicular to OA and then any line parallel to the torque line AC'. This parallel intercepts OK at J giving the measure HJ as unity slip. Consequently from any operating point P on the circle the interception of PA with HJ provides the corresponding slip at Z.

#### 4.2.5 Construction of the "Exact" Circle Diagram from Test Data

The exact circle diagram can be constructed from test data as follows: Let

$I_{NL}$  = measured value of no-load current per phase

$I_{SC}$  = primary short circuit current per phase for  
full rated voltage calculated from the results  
of a short circuit test at reduced voltage

$\cos \psi_{NL}$  = power factor at no-load

$\cos \psi_{SC}$  = power factor at short circuit measured at  
reduced voltage

Figure 4.7 Determination of Performance

$R_1$  = primary resistance per phase measured at working temperature.

In Figure 4.8 OA represents  $I_{NL}$  in magnitude and phase. One can draw the horizontal AY. The centre of the circle lies on the line AC making an angle  $2\alpha$  with AY. The angle  $\alpha$  can be calculated from

$$\alpha \approx \sin^{-1} \frac{|I_{NL}| R_1}{V_1}$$

Now joining AK and constructing the perpendicular bisector of AK such that it intersects the line AC at a point M, then M is the centre of the locus of  $I_1$  so that it can be drawn with the radius MA. By reference to Figure 4.3 one obtains

$$|E_{NL}| \cos \theta_m = V_1 \cos \theta_{NL} - |I_{NL}| * R_1$$

$$\theta_m = \phi_{NL} + \alpha$$

$E_{NL}$  can be calculated and from this

$$Z_m = \frac{E_{NL}}{I_{NL}}$$

The vector AB in Figure 4.8 can now be drawn in magnitude equal to  $(Z_1/Z_m) * CA$  and making an angle  $(\theta_m - \theta_1)$  clockwise relative to the direction of CA. Then AB is the diameter of the circular locus of  $I_m$  and the circle diagram can be completed as in Figure 4.6.

The results of the tests mentioned in the previous section for constructing the circle diagram are given in Table 4.1.

|                          |                         |                           |
|--------------------------|-------------------------|---------------------------|
| $I_{NL} = 5.75$ amperes  | $\cos \psi_{NL} = 0.19$ | $\psi_{NL} = 79^\circ$    |
| $I_{SC} = 50.60$ amperes | $\cos \psi_{SC} = 0.41$ | $\psi_{SC} = 65.40^\circ$ |
| $R_1 = 0.40$ ohms        | $X_1 = 1.08$ ohms       | $\theta_m = 80^\circ$     |
| $CC' = 8.32$ amperes     | $\alpha = 1.10^\circ$   | $\theta_1 = 69.40^\circ$  |

Table 4.1 Tabulation of Test Data

Figure 4.14 shows the constructed circle diagram from the test results given in Table 4.1. The interpretation of the results are given in Section 4.8.

#### 4.3 The Second Method of Determining the "Exact" Circle Diagram

The circle diagram can also be derived from the equivalent circuit in Figure 4.1 and by the method of inversion according to [21].

##### 4.3.1 Inversion

If the equivalent circuit of an electrical machine is expressed in the form of a series-parallel network of impedances, then the total circuit current at constant voltage can be obtained by finding the locus of the combined admittance between terminals. For this purpose

Figure 4.8 Construction of the Circle Diagram from Test Data

parallel branches of the network are added as admittances, and series branches as impedances. To find the admittance of a branch from its impedance involves the inversion of the latter since

$$Y = y \angle -\theta = \frac{1}{Z} = \frac{1}{Z} \angle \theta$$

The process is simplified when simple geometrical loci have to be inverted, and for the present purpose it is sufficient to note:

(a) The inverse of a straight line AB about a pole O, Figure 4.9(a), is a circle passing through O with a diameter on the perpendicular OC from O to AB.

(b) The inverse of a circle about a pole on its circumference is a straight line perpendicular to the diameter of the circle through O. This is the converse of (a).

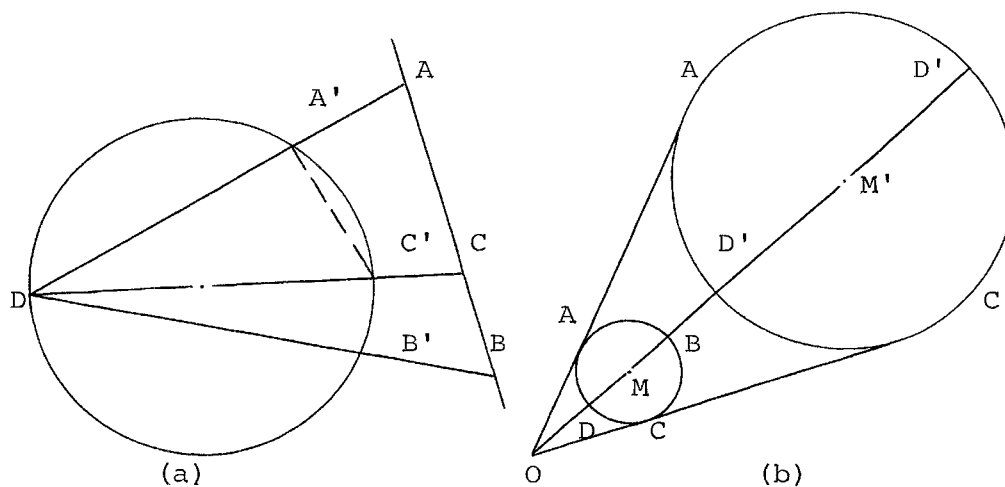


Figure 4.9 Inversion of Straight Line and Circle

(c) The inverse of a circle about any point not on its circumference is another circle with its centre on the line joining the centre of the inversion  $O$  to the centre  $M$  of the circle and included between the same tangents, Figure 4.9(b). The rotation of the points on the two circle is in opposite sense. These rules are geometrical. For electrical purposes, admittance is obtained from impedance by reflection across the axis of resistance or conductance.

#### 4.3.2 The Impedance Diagram

The usual equations representing an induction motor can be written in the complex notation from the equivalent circuit in Figure 4.1 as follows:

$$\begin{aligned}\bar{V}_1 &= (R_1 + jX_1)\bar{I}_1 + jX_M \bar{I}_2 \\ \bar{V}_2 &= jX_M s\bar{I}_1 + (R_2 + jX_2 s)\bar{I}_2\end{aligned}\tag{4.21}$$

For a non-zero slip and the rotor short-circuited one can easily derive from (4.21) the complex impedance referred to the stator

$$\bar{Z}_1 = \frac{\bar{V}_1}{\bar{I}_1} = R_1 + jX_1 + \frac{X_M^2}{\frac{R_2}{s} + jX_2}$$

When the slip varies the extremity of  $Z_1$  is a circle according to [22]. It can easily be demonstrated that the

diameter of the circle is given by the points  $s = 0$  and infinity. Corresponding values for stator impedance are

$$\overline{Z}_1(0) = R_1 + jX_1 \quad (4.22)$$

$$\overline{Z}_1(\infty) = R_1 + j\sigma X_1 \quad (4.23)$$

where  $\sigma$  is the mean leakage factor also called Blondel coefficient and defined with the mutual inductance  $M$  as

$$M^2 = (1 - \sigma) L_1 L_2$$

Figure 4.10 shows the impedance diagram obtained from equations (4.22) and (4.23).

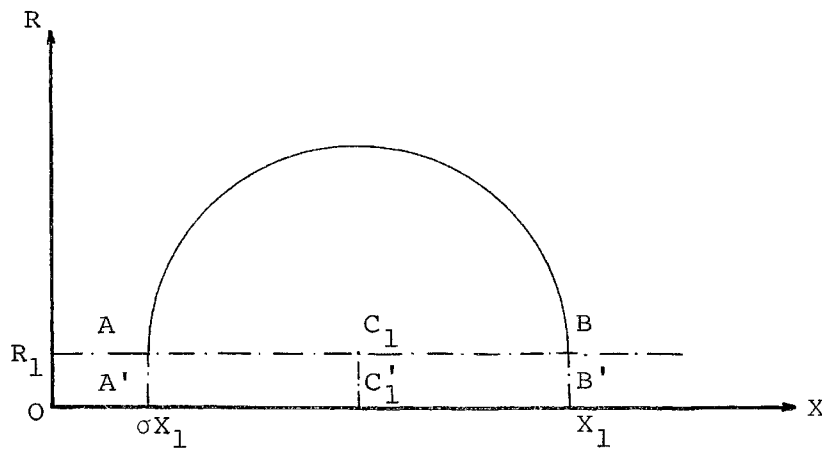


Figure 4.10 The Impedance Diagram



The coordinates of the centre  $C_1$  are

$$\begin{aligned} X_{C_1} &= OA' \left( \frac{1 + \sigma}{2\sigma} \right) = \left( \frac{1 + \sigma}{2} \right) X_1 \\ Y_{C_1} &= R_1 \end{aligned} \quad (4.24)$$

The point corresponding to  $s = 1$  can be calculated as follows:

$$\begin{aligned} \overline{Z}_1(1) &= R_1 + jX_1 + \frac{X_m^2}{R_2 + jX_2} \\ &= \frac{(R_1 + jX_1)(R_2^2 + X_2^2) + (1 - \sigma) X_1 X_2 (R_2 - jX_2)}{R_2^2 + X_2^2} \end{aligned}$$

#### 4.3.3 The Admittance Diagram

The impedance diagram is not as easy to use as the admittance diagram. Henceforth, the impedance diagram has to be inverted. For commodity the pole of inversion is chosen to be the origin and the power of inversion  $V_1$ . This provides automatically the ampere scale for the admittance diagram since

$$\frac{1}{\overline{Z}_1} = \frac{\overline{I}_1}{\overline{V}_1} = \frac{R_2 + jX_2 \cdot s}{(R_1 + jX_1)(R_2 + jX_2 s) + sX_m^2} \quad (4.25)$$

One can write from Figure 4.10

$$\begin{aligned} AC_1 &= r \text{ radius of the impedance circle} \\ &= \frac{1 - \sigma}{2} X_1 \end{aligned} \quad (4.26)$$

and the power of the origin to the circle is

$$p_1 = (OC_1 - r)(OC_1 + r) = OC_1^2 - r^2 \quad (4.27)$$

besides by triangulation

$$OC_1^2 = (OC_1')^2 + (C_1'C_1)^2 = R_1^2 + \left(\frac{1+\sigma}{2} x_1\right)^2 \quad (4.28)$$

The combination of equations (4.26), (4.27) and (4.28) gives

$$p_1 = R_1^2 + \sigma x_1^2 \quad (4.29)$$

From the general properties derived for the inversion in Section 4.3.1 follows that the inverse of a circle ( $C_1$ ) when the pole (O) is not on the circle is another circle ( $C_2$ ). Furthermore the line joining the centres of the two circles will be passing through the pole of inversion as shown on Figure 4.11(b).

If a straight line through (O) intersects the circle at A, B, D and C, by the definition of the transformation the power of inversion with pole (O) allows to write

$$p = OA \cdot OC \quad (4.30)$$

where p is chosen to be  $V_1$ .

Furthermore the power of the point (O) to the circle ( $C_1$ ) is by definition

$$p_1 = OA \cdot OB \quad (4.31)$$

Hence the ratio of powers gives

$$\frac{p}{p_1} = \frac{OC}{OB} \quad (4.32)$$

The circles related by inversion are also homothetic.

Therefore

$$\frac{OC}{OB} = \frac{OC_2}{OC_1} = \frac{p}{p_1} \quad (4.33)$$

Projecting  $OC_1$  on the axis gives the relations between X and Y coordinates of the centres as

$$\frac{p}{p_1} = \frac{Y_{C_2}}{Y_{C_1}} = \frac{X_{C_2}}{X_{C_1}} \quad (4.34)$$

Substituting the values of  $Y_{C_1}$ ,  $X_{C_1}$ ,  $p$  and  $p_1$  in the equation (4.34) gives

$$\frac{Y_{C_2}}{R_1} = \frac{\frac{X_{C_2}}{(1 + \sigma)X_1}}{\frac{2}{2}} = \frac{V_1}{R_1^2 + \sigma X_1^2} \quad (4.35)$$

However, one can use the no-load test identity

$$V_1^2 = (R_1^2 + X_1^2) I_{NL}^2 \quad (4.36)$$

where  $I_{NL}$  is the no-load stator current, to obtain

$$X_1^2 = \left( \frac{V_1}{I_{NL}} \right)^2 - R_1^2 \quad (4.37)$$

and by combining the equations (4.37) and (4.35) the coordinates of the centre of the admittance diagram are found to be

$$Y_{C_2} = \frac{V_1 R_1}{R_1^2 (1 - \sigma) + \sigma \left( \frac{V_1}{I_{NL}} \right)^2} \quad (4.38)$$

$$X_{C_2} = \frac{V_1 (1 + \sigma) \sqrt{\left( \frac{V_1}{I_{NL}} \right)^2 - R_1^2}}{2 [R_1^2 (1 - \sigma) + \sigma \left( \frac{V_1}{I_{NL}} \right)^2]} \quad (4.39)$$

In case of  $R_1 \ll \sigma X_1^2$  one obtains from the above equations

$$Y_{C_2} \approx \frac{R_1 I_{NL}^2}{\sigma V_1} \quad (4.40)$$

$$X_{C_2} \approx \frac{1 + \sigma}{2\sigma} \cdot \frac{I_{NL}^2}{V_1} \sqrt{\left( \frac{V_1}{I_{NL}} \right)^2 - R_1^2} \quad (4.41)$$

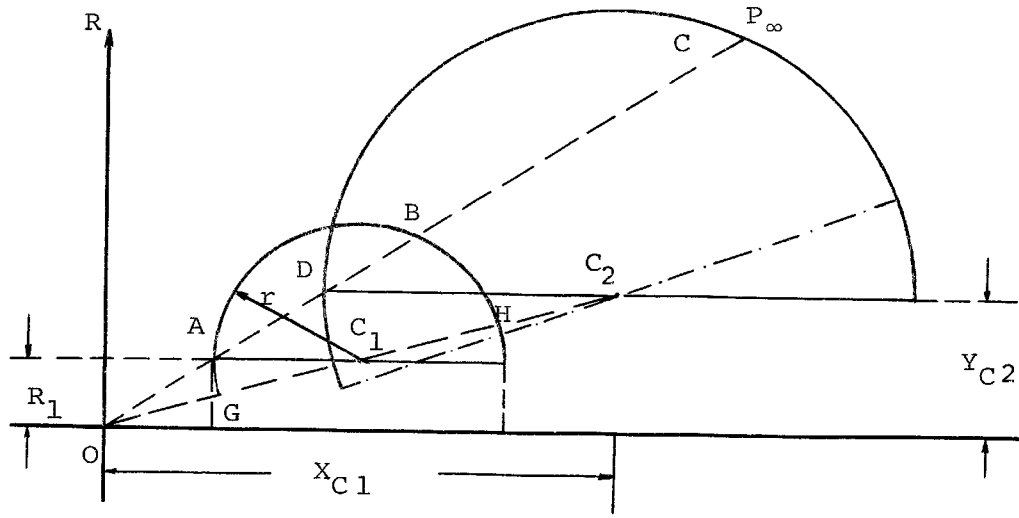
#### 4.4 Determination of the Parameters of the Circle Diagram

The stator resistance, the no-load current and the leakage coefficient are the only parameters needed for the centre.  $R_1$  and  $I_{NL}$  are very easily obtained.

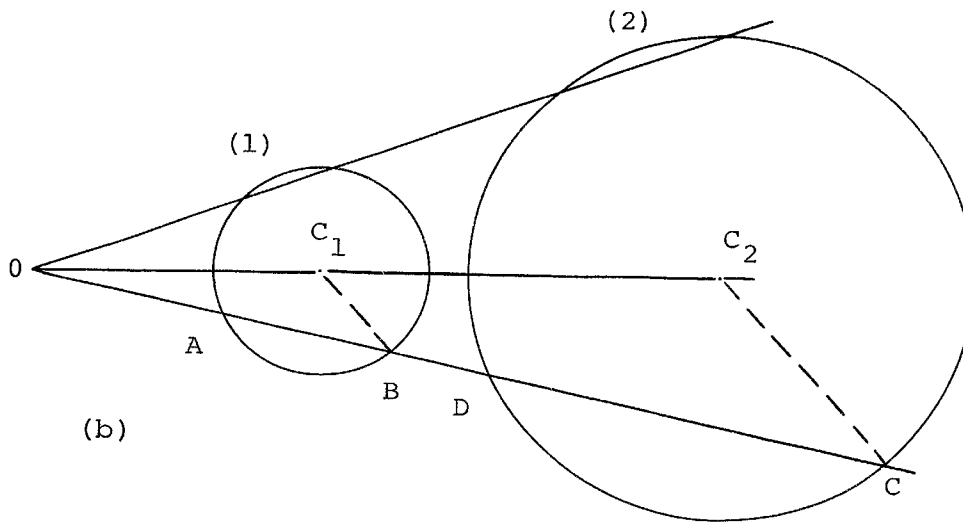
##### 4.4.1 Measurement of Blondel's Coefficient

###### (a) First method for wound rotors only

Energize the stator with the nominal voltage  $V_1$  and



(a)



(b)

Figure 4.11 Inversion of Impedance to Admittance Diagram

measure the open-circuited rotor voltage  $V_{2(oc)}$ . The transformation ratio  $N_1$  can be written from equation (4.21) as

$$N_1 = \frac{V_{2(oc)}}{V_1} = \frac{jX_m}{R_1 + jX_1} \quad (4.42)$$

Likewise energize the rotor with a voltage  $V_2$  and read the open-circuited stator voltage  $V_{1(oc)}$  and write the transformation ratio  $N_2$  as

$$N_2 = \frac{V_{1(oc)}}{V_2} = \frac{jX_m}{R_2 + jX_2} \quad (4.43)$$

In a first approximation one can state that the reactances are always much larger than the winding resistances hence combining equations (4.41) and (4.42)

$$N_1 N_2 \approx \frac{X_m^2}{X_1 X_2} = 1 - \sigma$$

Therefore

$$\sigma = 1 - N_1 N_2 \quad (4.44)$$

The only precaution should be to find a rotor voltage which will as nearly as possible give the same flux condition as does the rated voltage applied to the stator. This obviously will never occur. However, one compromise would be to create an equal mean flux condition in the two cases.

If one applies a rotor excitation voltage which will give a stator open-circuit voltage equal to the first case  $V_1$ , then the mean flux condition is fairly well approached.

(b) General Case

Unfortunately the previous method did not take the motor under running conditions and the flux distribution altered. The following method to obtain the leakage factor has been derived from the theory of single phase motors [21].

It can be shown using the symmetrical components of a single phase motor that a three phase induction machine, running on two phases only, will rebuild the third voltage to a magnitude of  $V$  as

$$\frac{U}{V} = \sqrt{3} \frac{1 + \sigma}{1 - \sigma}$$

where  $U$  is the rated voltage between the two other phases. Hence from this simple experiment one can deduct  $\sigma$  as

$$\sigma = \frac{U - \sqrt{3} V}{U + \sqrt{3} V} \quad (4.45)$$

This method has the advantage of including any kind of rotors, but provides only the no-load leakage factor.

#### 4.5 Influence of the No-Load Losses

The no-load losses consist of the stator copper loss  $I^2R$ , friction and windage loss, denoted as the mechanical loss  $P_m$  and the stator core loss  $P_{fs}$ . Figure 4.13

demonstrates these losses. The no-load mechanical loss  $P_m$  is approximately constant in the region to be investigated. Therefore the real motor torque is obtained by subtracting the torque corresponding to the mechanical loss from the theoretical torque. Thus on the circle diagram the line which represents the delivered mechanical power should be shifted up by an amount  $P_m$ .

The stator core loss  $P_{fs}$  at no-load represents a certain amount which does not affect the circle diagram. It merely shifts the origin  $O$  by  $\overline{OO'}$  representing  $P_{fs}$ .

In Figure 4.13,  $OP_{NL}$  denotes the actual and  $OP_O$  the ideal no-load current.

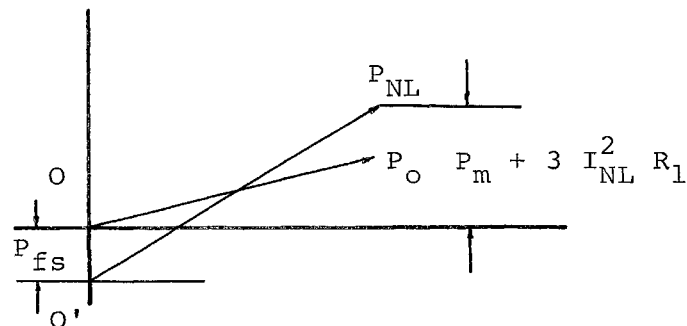


Figure 4.12 Separation of No-Load Losses

#### 4.6 Construction of the Exact Circle Diagram from Test Data

The exact circle diagram can be constructed from test data as follows:



Let  $I_{NL}$  = measured value of no-load current per phase

$X_C$  = X-coordinate of the centre of the circle

$Y_C$  = Y-coordinate of the centre of the circle

$\cos \psi_{NL}$  = power factor at no-load.

The parameters  $X_C$  and  $Y_C$  are to be calculated from equations (4.37) and (4.38).

Figure 4.13 shows the constructed circle diagram from the above data. The no-load losses are separated and the origin  $O'$  is shifted up to the point  $O$  by the amount  $P_{fs}$ . From reduced voltage test with blocked rotor the primary short circuit-current can be obtained and carried out in Figure 4.13 as  $\overline{OP}_{SC}$  on the circle in magnitude and phase.

Since in all conventional induction machines the no-load slip is very close to zero, the no-load point and the ideal zero slip point are undistinguishable on the diagram. Therefore the lines for developed and delivered mechanical power are the same at these points. For theoretical zero slip the rotor runs synchronously with the rotating flux and the rotor current is zero. This can be achieved only if the rotor is brought up to synchronous speed by another machine, and this machine will have to supply the mechanical losses of the rotor, i.e. the friction and windage losses, and core loss. The active component of the stator current at  $s = 0$  is smaller than that at no-load by the amount corresponding to these losses. The point on the circle

which corresponds to  $s = 0$  will be denoted by  $P_0$ . At zero slip the developed mechanical power is also zero. The point corresponding to  $s = 1$  is denoted by  $P_{SC}$ , where the mechanical power delivered to the shaft is zero. Therefore the delivered mechanical power line is obtained with good approximation by  $\overline{P_0 P_{SC}}$ .

#### 4.7 Calculation of Coordinates of Point $P_\infty$

At theoretical infinite slip the coordinates of the point  $P_\infty$  can be calculated as follows:

From equation (4.33) one obtains

$$\frac{OC_2}{OC_1} = \frac{p}{p_1} = \frac{OD}{OA} \quad (4.46)$$

Looking at Figure 4.11(a) which shows the relation between the two diameters, then the equations (4.33) and (4.46) allow to write

$$OD = OA \frac{OC_2}{OC_1} = OA \frac{Y_{C_2}}{Y_{C_1}} \quad (4.47)$$

From equation (4.30) one obtains

$$OC = \frac{p}{OA} \quad (4.48)$$

The combination of (4.47) and (4.48) gives

$$\frac{OC}{OD} = \frac{p}{OA^2} \cdot \frac{Y_{C_1}}{Y_{C_2}} \quad (4.49)$$

But one can write from Figure 4.11(a)

$$\frac{OC}{OD} = \frac{Y_{P_{\infty}}}{Y_{C_2}} \quad (4.50)$$

Therefore  $Y_{P_{\infty}}$  can be calculated from equations (4.49) and (4.50) as

$$Y_{P_{\infty}} = p \frac{Y_{C_1}}{OA^2} \quad (4.51)$$

Now  $OA^2$  can be obtained from (4.23) as

$$OA^2 = z_{1(\infty)}^2 = R_1^2 + \sigma^2 x_1^2 \quad (4.52)$$

$x_1^2$  has been calculated from (4.36) as

$$x_1^2 = \left( \frac{V_1}{I_{NL}} \right)^2 - R_1^2$$

Substitution of the value of  $x_1$  in (4.52) yields

$$z_{1(\infty)}^2 = R_1^2 (1 - \sigma^2) + \sigma^2 \left( \frac{V_1}{I_{NL}} \right)^2 \quad (4.53)$$

Therefore the ordinate of point  $P_{\infty}$  is found to be

$$Y_{P_{\infty}} = \frac{p Y_{C_1}}{R_1^2 (1 - \sigma^2) + \sigma^2 \left( \frac{V_1}{I_{NL}} \right)^2} \quad (4.54)$$

Similarly for the abscissa of the point  $P_\infty$  one obtains from equation (4.33) and Figure 4.11(a)

$$\frac{X_{P_\infty}}{\sigma X_1} = \frac{OC_2}{OC_1} = \frac{p}{OA^2} \quad (4.55)$$

$$X_{P_\infty} = \sigma X_1 \frac{p}{OA^2},$$

and finally with respect to (4.37) one obtains

$$X_{P_\infty} = \sigma \frac{p}{OA^2} \left( \frac{V_1}{I_{NL}} \right)^2 - R_1^2 \quad (4.56)$$

where  $OA^2$  is given in (4.52).

From Figure 4.13 the machine performance could be obtained as below:

|                          |   |
|--------------------------|---|
| $AK \sim P_1$            | primary power input                     |
| $AC \sim P_{rot.f}$      | power transferred by the rotating field |
| $AC \sim T_{dev.}$       | developed torque                        |
| $AB \sim P_{m,del.}$     | mechanical power delivered at the shaft |
| $CK = (AK - AC)$         | primary copper loss and core            |
| $\sim (P_1 - P_{rot.f})$ | loss due to the main flux and           |
| $= 3 I_1^2 R_1 + P_{fs}$ | friction and windage loss               |
| $+ P_m$                  |   |
| $CT = 3 I_1^2 R_1$       | stator copper loss                      |



|                                 |                           |
|---------------------------------|---------------------------|
| $TD \sim P_{fs}$                | stator core loss          |
| $DK \sim P_m$                   | friction and windage loss |
| $CB = (AC-AB)$                  | secondary copper loss     |
| $\sim (P_{rot.f} - P_{m del.})$ |                           |
| $= 3 I_2^2 R_2$                 |                           |
| $\eta = \frac{AB}{AK}$          | efficiency of the machine |

The scale of slip can be obtained by drawing  $HP_0$  perpendicular to  $OP_0$  and then any line parallel to the torque line  $OP_\infty$ .

This parallel intercepts  $OP_{SC}$  at J giving the measure HJ as unity slip. Consequently from any operating point A on the circle the interception of  $P_0A$  with HJ provides the corresponding slip at Z.

#### 4.8 Examples of Measurements and Interpretation of Results

The results of the test mentioned in previous sections are given in Table 4.2.

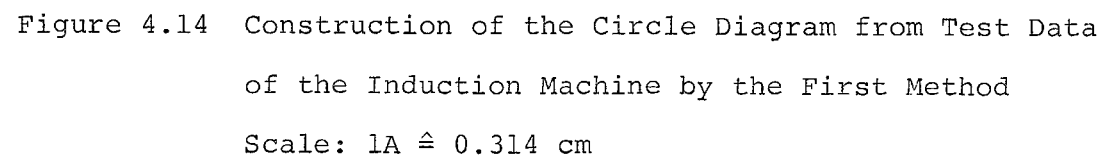
Figure 4.15 shows the constructed circle diagram from the test results given in Table 4.2.

The results of the circle diagram readings are compared to standard I.E.E.E. test code procedure and experimentally measured results. The torque-slip characteristic is shown on Figure 4.16 and the circle diagram seems to fit the standard results very closely. Figure 4.17 depicts the stator current versus slip curves and proves in both

cases to be accurate enough. For input power versus slip on Figure 4.18 and power factor predictions on Figure 4.19 both methods prove themselves close enough for all practical purposes.

| Blondel Coefficient  |   |
|--|---|
| $V_1 = 196$ (Volts)<br>$V_{2(oc)} = 221$ (Volts)   | $V_{1(oc)} = 196$ (Volts)<br>$V_2 = 246.50$ (Volts) |
| $N_1 = \frac{V_{2(oc)}}{V_1} = \frac{221}{196}$ $N_2 = \frac{V_{1(oc)}}{V_2} = \frac{196}{246.50}$ $\sigma = 1 - N_1 N_2 = 1 - \frac{221}{246.50} = 0.103$ |   |
| Coordinates of the Centre<br>of Admittance Diagram   | $X_C = 31.33$ (Amperes)<br>$Y_C = 1.07$ (Amperes)   |
| Coordinates of Point<br>$P_\infty$   | $X_P = 55.40$ (Amperes)<br>$Y_P = 23$ (Amperes)     |
| No-Load Test   |   |
| $I_{NL} = 5.75$ (Amperes)<br>$\cos \psi_{NL} = 0.19$   | $P_m = 216$ (Watts)<br>$P_{fs} = 176$ (Watts)       |
| Short-Circuit Test   |   |
| $I_{SC} = 50.60$ (Amperes)   | $\cos \psi_{SC} = 0.41$                             |

Table 4.2 Tabulation of Test Data







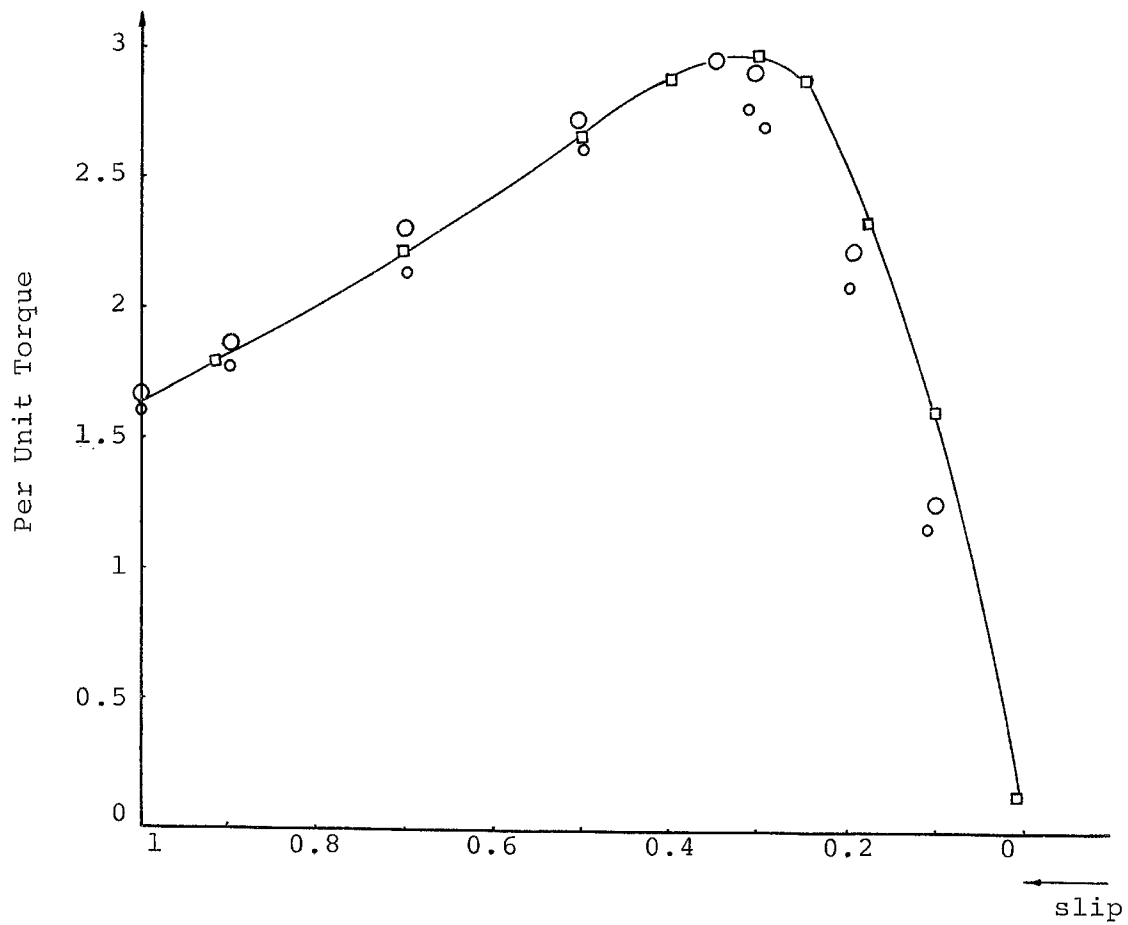


Figure 4.16 Per Unit Torque versus Slip

○ ○ ○ Circle Diagram First Method

○ ○ ○ Circle Diagram Second Method

□ — □ — □ I.E.E. Test Code, Stray Losses Included

Base Torque = 15 ft-lb

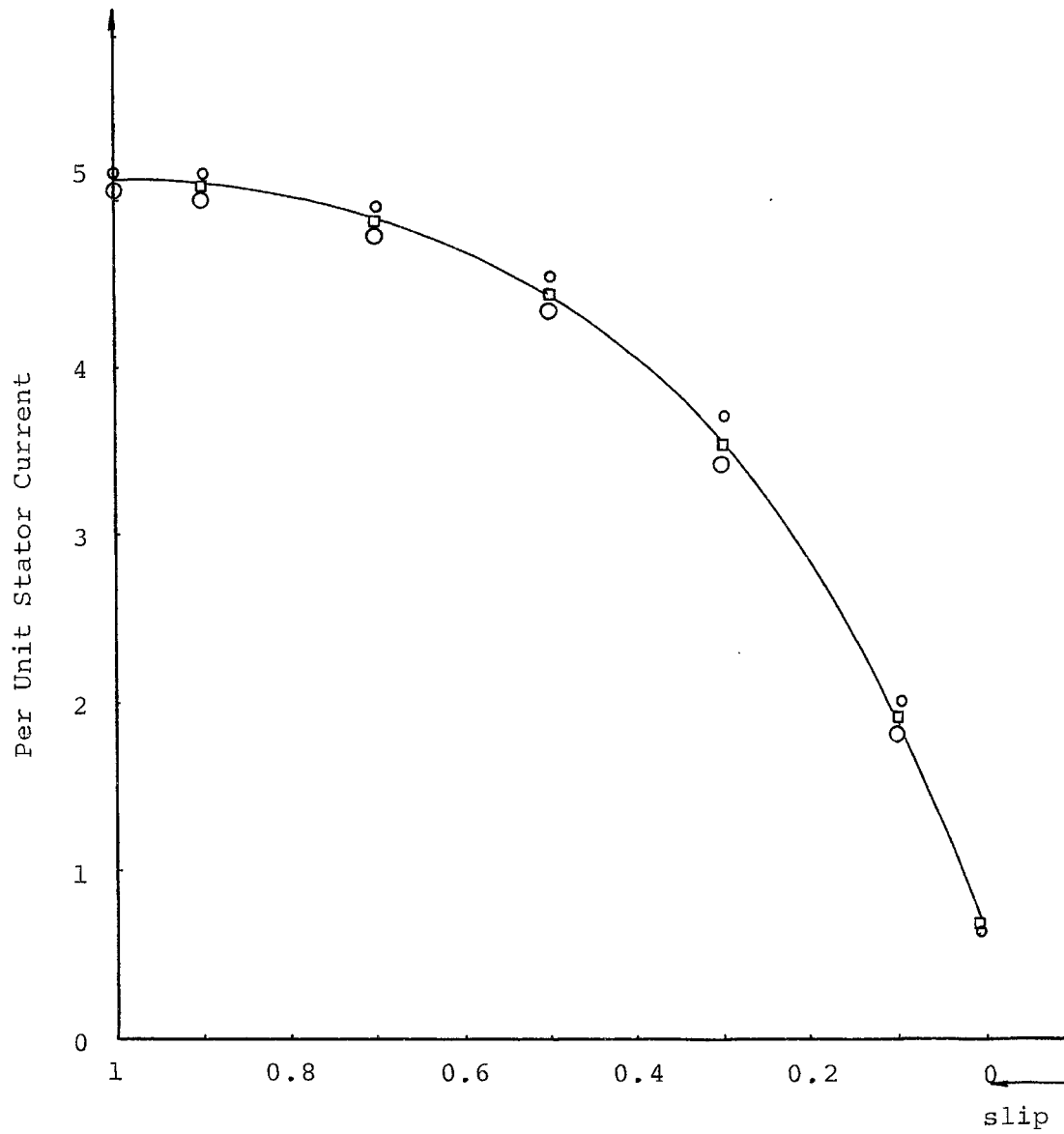


Figure 4.17 Per Unit Stator Current versus Slip

○ ○ ○ Circle Diagram Second Method

○ ○ ○ Circle Diagram First Method

□ — □ — □ I.E.E.E. Test Code

Base Stator Current = 10A

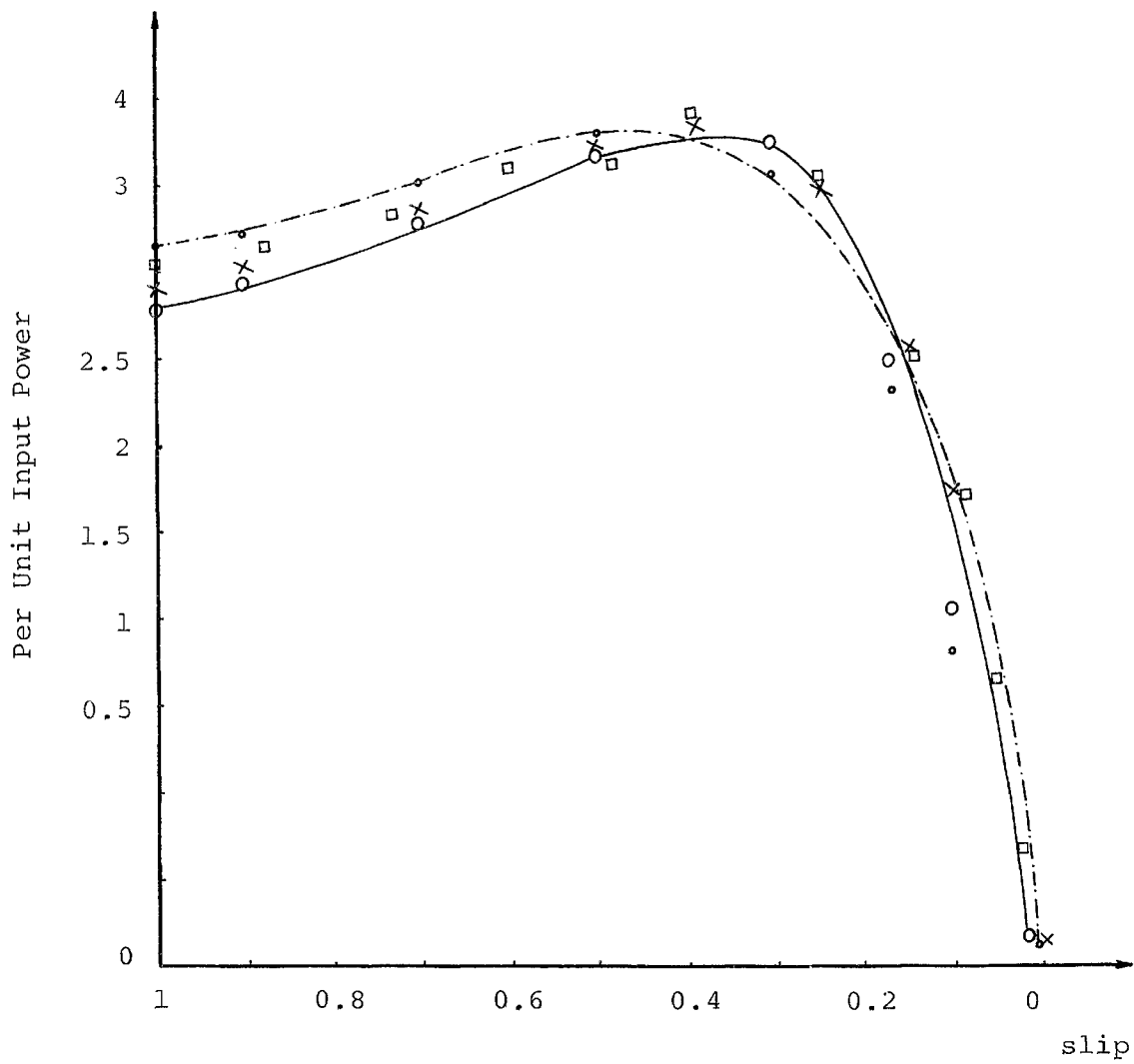


Figure 4.18 Per Unit Input Power versus Slip

○ — ○ — ○ Circle Diagram Second Method

○ — ○ — ○ Circle Diagram First Method

□ □ □ Measured

× × × I.E.E.E. Test Code

Base Input Power = 2904 W

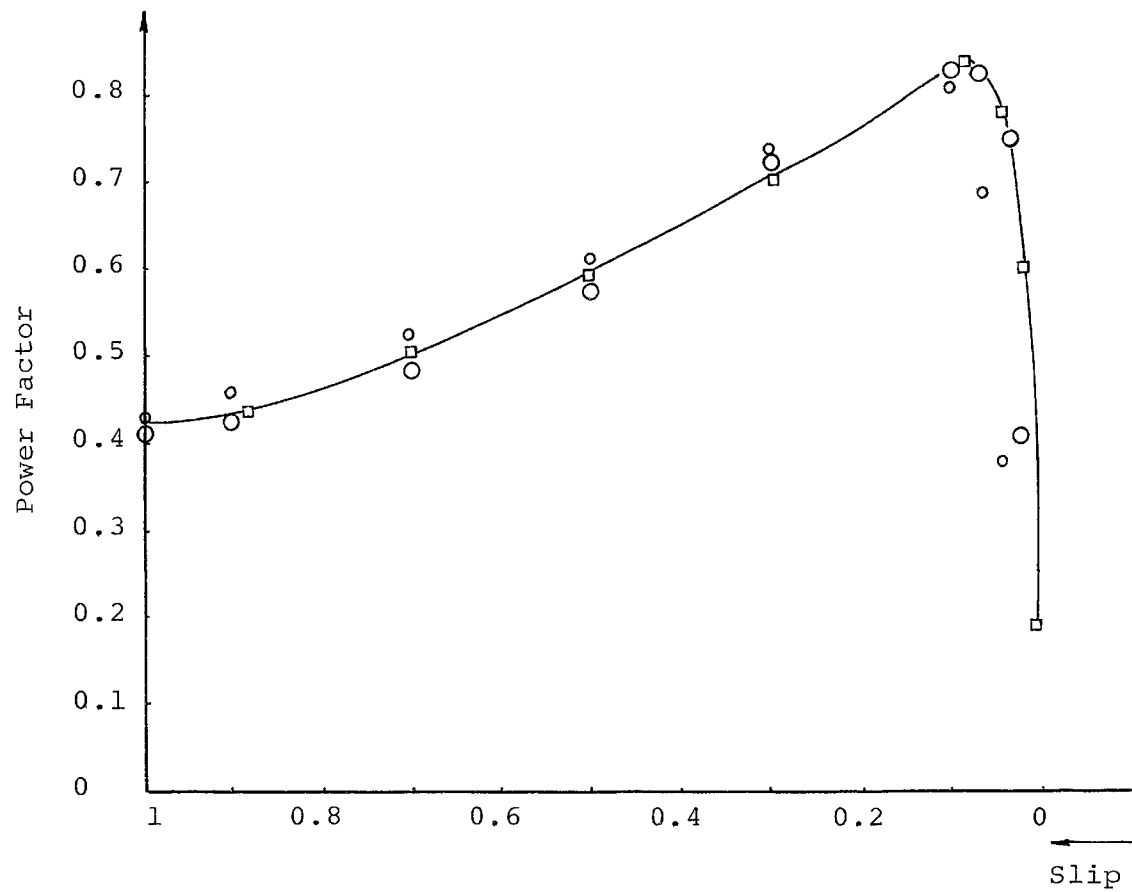


Figure 4.19 Power Factor versus Slip

○ ○ ○ Circle Diagram Second Method

○ ○ ○ Circle Diagram First Method

□ □ □ I.E.E.E. Test Code

## CHAPTER 5

### SUMMARY AND CONCLUSION

#### 5.1 Summary

This report was undertaken to investigate the stray losses due to the higher harmonics and to study the circle diagram of the induction motors, using more accurate methods for drawing it.

The performance of the machine under test was determined according to the I.E.E.E. "Test Code Procedure". The stray losses were measured by using the reverse rotation, standstill, no-load and Rawcliffe and Menon tests and the extrapolation of these losses with current and speed variation was done according to the I.E.E.E. test procedure.

The output torque, input power and current were measured at several slip points over the speed range. The suggested expression for computing torque according to the I.E.E.E. test code [15] was found to be inaccurate. Therefore, torque calculations were carried out using the method suggested in [16]. This expression was found to give good agreement between measured and calculated torque.

From the results of measurement and calculation, curves of developed torque, input current, power factor

and input power were plotted. The calculated torque-slip curve was plotted with and without the effects of stray loss. The air-gap flux of the machine was recorded at no-load, half-load and full-load on a magnetic tape, and analysed by means of a discrete Fourier transform with piecewise approximation. The harmonics content in the air-gap flux allowed the determination of the harmonic losses as a part of the total stray load losses.

Two methods of drawing circle diagram were explained. The curves of developed torque, input current, power factor and input power of both methods were plotted and their results were compared with those obtained from the I.E.E.E. test code procedure.

## 5.2 Conclusion of First Part

As a result of the investigation, the stray load losses could be classified in those of eddy-current and iron losses at the supply frequency, tooth ripple in the main and tooth ripple in the zigzag leakage flux produced by the magnetizing current. The latter includes the stray losses due to the harmonics. A paper by Barton and Ahmad [14] maintains that these losses could be separated by three tests, standstill, Rawcliff and Menon, and reverse rotation tests. As the results of the experiments in this work show no-load, standstill and reverse rotation tests are sufficient together with the extrapolation of

the results of the reverse rotation test according to the equation (3.1)

$$P_{st} = H \left( \frac{n_o}{n_s} \right)^{1.6} \left( \frac{I_1}{I_r} \right)^{1.9}$$

to predict the total stray losses over the whole practicable speed range. The Rawcliffe and Menon test was considered as only a graphical method derived from no-load test which showed, because of the graphical extrapolation, not to be as accurate as the no-load test. The Ware's test which is accepted by I.E.E.E. test code for measuring the stray losses at the fundamental frequency requires the removal of the rotor, and hence was considered as an impractical procedure. The standstill and no-load tests were considered to yield the same result and were performed because of their simplicity. A comparison of the results obtained from the reverse rotation test and the extrapolation with the current and speed for the variation of  $I_r$ , the stator winding current during the stray loss test, from three-quarter to one and one-half times rated current, shows that the value of the stray loss up to the rated stator current remains within the same range in both cases, but increases by reverse rotation test rapidly for higher values than the rated stator current. Therefore it is realistic to assume that the reverse rotation test is an adequate method for the determination of the stray losses associated with the zigzag leakage flux from the slips



greater than the no-load slip up to the full-load slip, i.e. within the actual working region of the machine. On the other hand the extrapolation with current and speed according to the equation (3.1) predicts with sufficient accuracy the stray losses due to the leakage flux of the magnetizing current in the remaining speed range. According to a paper [12] by Barton and Ahmad, for fractional slips exceeding 0.05, the stray loss associated with the zigzag leakage flux predominates over that with the main flux. It was observed in the machine under test that the actual and principal source of the stray losses at slips greater than the full-load slip was due to the high frequency variations in the component of tooth flux produced by the zigzag leakage. From the reverse rotation test the stray loss due to the leakage flux was obtained accurately, only for all slips between the no-load and full-load, therefore the extrapolation with current and speed according to the equation (3.1) remains as the only means for determination of the total stray losses in the remaining speed range. The torque-slip curve of the machine under test with the stray loss obtained from the equation (3.1), Figure 3.5, for the whole speed range was plotted.

The component of the total harmonic losses due to the tooth ripple in the main field flux was found to be significant within the working range of the induction

machine under test. In the case of no-load this was about 45 percent of the total harmonic losses and at half-load and full-load nearly 30 percent. Harmonic analysis of the air-gap flux shows to give sufficient information about the percentage of the harmonic losses in the total stray losses of the machine.

Two sources of errors which may influence the results were observed during the reverse rotation test. An accurate value of stator resistance is essential as stator  $I^2R$  comprise a large percentage of the total power measured. The present I.E.E. test code specifies that the stator  $I^2R$  losses shall be determined at "test temperature" but leaves the determination of the test temperature to the discretion of the tester. Since an error in the stator resistance reflects directly in the stray load loss, it is suggested that the following be incorporated into the test code.

1) In Section 20-4.3.4.2, the word "resistance" should replace the word "temperature" in the sentences: "The electrical input minus the stator  $I^2R$  loss at test resistance is equal to the fundamental frequency stray-load loss".

2) In Section 20-4.3.4.2.3, "The stator winding  $I_t^2(R)$  loss shall be taken at each load point", with other words: The resistance has to be taken at each load point.

The second source of error was caused by the core losses due to the main field flux. These losses composed of tooth frequency losses due to the ripples in the main field flux, are present during the reverse rotation test but not accounted for in the calculations outlined by the test code. These could be determined under each load condition, preferably within the working range of the machine, by using the harmonic analysis of the main-flux and calculating the higher harmonic losses.

The harmonic analysis of the air-gap flux is an effective method which allows the design engineer to obtain information regarding the field characteristics in all types of induction machines, and therefore to eliminate those harmonics which contribute to the higher harmonic losses.

### 5.3 Conclusion of Second Part

By introduction of a complex  $K$  the exact circle diagram can be constructed from an equivalent simplified circuit described in Section 4.2.2. This method can also be applied to induction motors with squirrel-cage rotors having eddy-current bars or with double cage rotors because the value of complex constant  $K$  is a function of the primary impedance  $Z_1$  and the magnetizing impedance  $Z_m$ , and is therefore independent of the form which the squirrel-cage rotor may take. The second method which is constructed from the exact equivalent circuit uses the method

of inversion and its properties. The coordinates of the centre of admittance circle and the point  $P_{\infty}$ , infinite slip, are calculated exactly. The performance predicted by this method fits the standard results very closely.

This close agreement is due to the following reasons:

Some authors have proposed practical ways of drawing the circle diagram [19, 22] from the results of the industrial plateform. Unfortunately, these parameters are available to the designer only, and the test results were leading to large graphical errors. The main point was that the centre of the admittance circle was obtained by intersect of two almost parallel lines, or better, using extrapolation which obviously is very impractical. The calculation of the centre and the point  $P_{\infty}$ , infinite slip, allows to obtain results accurate enough for all industrial purposes.

This method can be extremely useful in predicting performance criteria like maximum output power  $P_{\max}$  or maximum torque  $T_{\max}$  when several parameters would change simultaneously, and it could be extended to a representation of induction machines at different frequencies.

## APPENDIX I

### SPECIFICATIONS OF MACHINE

Manufacturer - Canadian General Electric

Horsepower - 3

Speed - 1200 r.p.m.

Wound Rotor

Frame - 254 H

Type - 17

Service Factor - 1.15

#### Stator Winding

Voltage - 208V line to line

77.8% pitch

Ampere - 10.5A

Pitch Factor - 0.9398

Number of Poles - 6, 60 Hz

3 Phase, 60° Phase Belt Width

54 Slots, 17 turns per coil

Distribution Factor - 0.96

Coil-span Slots 1 to 8

Connection - 2 circuit Y

#### Rotor Winding

Voltage - 260V line to line

3 Phase, 60° Phase Belt Width

Number of poles - 6

Distribution Factor - 0.966

36 Slots, 14 turns per coil

Connection - 1 Circuit Y

Coil-span Slots 1 to 7

100% pitch

Pitch Factor - 1.00

## APPENDIX II

### DISCRETE FOURIER SERIES

#### II.1 Trigonometric Fourier Series

A periodic function  $f(t)$  can be represented in terms of its Fourier components as

$$f(t) = a_0 + \sum_{n=1}^{\infty} (a_n \cos n \omega_0 t + b_n \sin n \omega_0 t) \quad (\text{II.1})$$

where

$$a_0 = \frac{1}{2\pi} \int_0^{2\pi} f(t) d(\omega t) \quad (\text{II.2})$$

$$a_n = \frac{1}{\pi} \int_0^{2\pi} f(t) \cos n(\omega t) d(\omega t) \quad (\text{II.3})$$

$$b_n = \frac{1}{\pi} \int_0^{2\pi} f(t) \sin n(\omega t) d(\omega t) \quad (\text{II.4})$$

#### II.2 Discrete Fourier Series

For the simplicity of the subsequent development set  $\omega t = X$ . Further, partition the interval  $0 \leq X \leq T$  into  $n$  parts. The function  $f(X)$  can now be approximated in  $i$ th partition (see Figure II.1) as

$$f(X_i) = AX_i + B, \quad i = 1, 2, \dots, n \quad (\text{II.5})$$

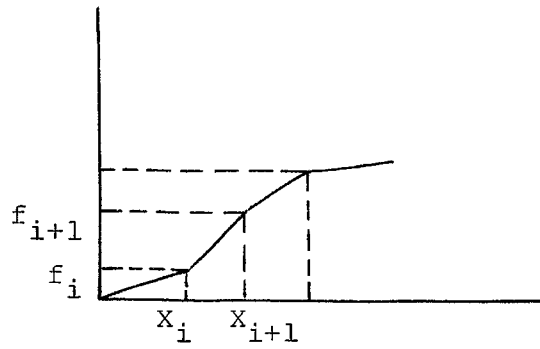


Figure II.1

Then equations (II.3) and (II.4) become

$$a_n = \frac{2}{T} \int_0^T (AX_i + B) \cos nX_i dX_i \quad (\text{II.6})$$

$$b_n = \frac{2}{T} \int_0^T (AX_i + B) \sin nX_i dX_i \quad (\text{II.7})$$

The integral  $\int (AX_i + B) \cos nX_i dX_i$  can be approximated as a combined sin- and cos-function which yields to

$$\int (AX_i + B) \cos nX_i dX_i = (AX_i + B) (C \sin nX_i + D \cos nX_i)$$

or

$$(AX_i + B) \cos nX_i = A(C \sin nX_i + D \cos nX_i) + C n(AX_i + B)$$

$$\cos nX_i - D n(AX_i + B) \sin nX_i \quad (\text{II.8})$$

Comparing the factors of trigonometric functions in equation (II.8) yields to

$$\int (AX_i + B) \cos nX_i dX_i = \frac{1}{n} (AX_i + B) \sin nX_i + \frac{A}{n^2} \cos nX_i \quad (\text{II.9})$$

Similarly

$$\int (AX_i + B) \sin nX_i \, dX_i = -\frac{1}{n}(AX_i + B) \cos nX_i + \frac{A}{n^2} \sin nX_i \quad (\text{II.10})$$

where the term A is the slope of the linear function  $f(X_i)$   
 $= AX_i + B$ .

Further this term is given by expression

$$A = \frac{f_{i+1} - f_i}{X_{i+1} - X_i} \quad (\text{II.11})$$

and

$$B = f_i - AX_i \quad (\text{II.12})$$

Thus with

$$I_{i+1} = \frac{1}{n}(AX_{i+1} + B) \cos(nX_{i+1}) + \frac{A}{n^2} \sin(nX_{i+1})$$

and

$$I_i = \frac{1}{n}(AX_i + B) \cos(nX_i) + \frac{A}{n^2} \sin(nX_i)$$

The area within the interval  $[X_i, X_{i+1}]$  is

$$\Delta_{i+1} = I_{i+1} - I_i \quad (\text{II.13})$$

The coefficient  $a_n$ , however, is calculated from equation (II.6), with respect to equations (II.9) and (II.13) as

$$a_n = \frac{2}{T} \sum_{i=0}^n \Delta_{i+1} \quad (\text{II.14})$$



where  $n$  is the number of intervals of linear approximated function  $f(X)$ .

For the coefficient  $b_n$  one similarly obtains the relationship as above from equations (II.7), (II.10) and (II.13).

It must be mentioned that the intervals need not be equal.

In order to reproduce the actual waveform the Fourier coefficients  $a_n$  and  $b_n$  have been computed according to equation (III.14). Hence

$$F(X) = \sum_{n=0}^{\infty} a_n f(X) + \sum_{n=1}^{\infty} b_n f(X) \quad (\text{II.15})$$

This approximation has been used to realize  $f(X)$  in discrete form.

## REFERENCES

1. Steinmetz, C.P. "The Alternating Current Induction Motor". A.I.E.E. Transactions, Vol. 14, pp. 185-223, 1897.
2. Dudley, A.M. "Stray Losses in Induction Motors". A.I.E.E. Transactions, Vol. 32, pp. 429-434, 1913.
3. Davis, R.W. "Notes on Induction Motor Losses". A.I.E.E. Transactions, Vol. 32, pp. 435-437, 1913.
4. Spooner, T. "Tooth Pulsation in Rotating Machinery". A.I.E.E. Transactions, Vol. 43, pp. 252-261, 1924.
5. Spooner, T. and Kinnard, I.F. "Surface Iron Losses with Reference to Laminated Materials". A.I.E.E. Transactions, Vol. 43, pp. 262, 1924.
6. Spooner, T. "Squirrel Cage Induction Motor Core Losses". A.I.E.E. Transactions, Vol. 44, pp. 32-37, 1925.
7. Spooner, T. "No-Load Induction Motor Core Losses". A.I.E.E. Transactions, Vol. 48, pp. 645-654, 1929.
8. Koch, C.J. "Measurement of Stray Load Loss". A.I.E.E. Transactions, Vol. 51, pp. 756-760, 1932.
9. Morgan, T.H. and Narbutouskih, P.M. "Stray Load Loss Test on Induction Machines". A.I.E.E. Transactions, Vol. 53, pp. 286-290, 1934.
10. Morgan, T.H. and Siegfried, V. "Stray Load Loss Tests on Induction Machines". A.I.E.E. Transactions, Vol. 55, pp. 493-497, 1936.
11. Morgan, T.H., Brown, W.E. and Schumer, A.J. "Reverse Rotation Test for the Determination of Stray Load Loss in Induction Machines". A.I.E.E. Transactions, Vol. 58, pp. 319-322, 1939.
12. Rawcliffe, G.H. and Menon, A.M. "A Simple Test for Harmonic-Frequency Losses in A.C. Machines". Proceedings I.E.E., Vol. 99, Pt. II, pp. 145-149, 1952.
13. Barton, T.H. and Ahmad, V. "Measurement and Prediction of Induction Motor Stray Loss at Large Slips". Proceedings I.E.E., Vol. 104, Pt. C, pp. 299-303, 1957.

14. Barton, T.H. and Ahmad, V. "The Measurement of Induction Motor Stray Loss and its Effect on Performance". Proceedings I.E.E., Vol.s 105-107, Pt. C, pp. 69-75, 1958-60.
15. Sattler, P.K. "Grundlagen der Elektrischen Maschinen" Institut fuer Elektrische Maschinen, Technische Hochschule Aachen, 1969.
16. Kovacs, K.P. "Betriebsverhalten von Asynchronmaschinen". VEB Verlag Technik Berlin, Chapter 4, 1957.
17. Langsdorf, A.S. "Theory of Alternating Current Machinery". McGraw-Hill Book Company, New York, Chapter X, 1939.
18. Ware, D.H. "Measurement of Stray Load Loss in Induction Motors". A.I.E.E. Transactions, Vol. 64, pp. 194-196, 1945.
19. Say, M.G. "The Performance and Design of Alternating Current Machines". Isaac Pitman & Sons, London, Chapter X, 1958.
20. Cheong, G.H. "The Exact Circle Diagram of the Induction Motor". I.E.E.E. Winter Power Conference, New York, 1973.
21. Pillet, E. "Machines à Induction". cours polycopiés, Ensekreg Grenoble, Tom IV, 1961.
22. Liwschitz, M. "D-C and A-C Machines based on Fundamental Laws". D. Van Nostrand Company, London, Chapter 27, 1952.

## CURRICULUM VITAE

Candidate's full name: Abdolmajid Banihaschemi

Schools attended (with dates): Hadaf 3 High School  
Teheran, 1955-1961

Universities attended (with dates and degrees obtained):

Technische Hochschule  
Aachen, W. Germany  
1963-1969  
Diplom Ingenieur  
(Electrical Engineering)